Catena 176 (2019) 125–144

Contents lists available at ScienceDirect

Catena

journal homepage: www.elsevier.com/locate/catena

Spatial and temporal variations in rainfall erosivity and erosivity density in South Korea

Ju-Young Shin[a], Taereem Kim[b], Jun-Haeng Heo[b], Joon-Hak Lee[c,*]

[a] National Institute of Meteorological Sciences, Seogwipo, South Korea
[b] Department of Civil and Environmental Engineering, Yonsei University, Seoul, South Korea
[c] Department of Civil Engineering and Environmental Sciences, Korea Military Academy, Seoul, South Korea

ARTICLE INFO

Keywords:
Correlation analysis
Erosivity density
Rainfall erosivity
Spatial analysis
Trend test

ABSTRACT

Rainfall erosivity is one of the key parameters in Universal Soil Loss Equation (USLE), which has been used to predict the amount of soil loss by water for 50 years. Investigating spatial and temporal trends in rainfall erosivity is important for soil and water conservation planning. Rainfall erosivity (the R factors) in many regions is expected to be altered due to changes in rainfall patterns related to rainfall intensity and the frequency and spatial distribution of storm events that may occur with climate change. In South Korea, some researchers have studied temporal variation in meteorological and hydrologic phenomena with climate change, particularly temperature and precipitation trends. The purpose of this study is to investigate spatial and temporal variations in rainfall erosivity and erosivity density and to improve our understanding of the evolution of rainfall erosivity in South Korea. First, we calculated rainfall erosivity at 46 stations for 1961–2015 using 5-min precipitation data. Second, we examined spatial and temporal variability in the rainfall erosivity; trends and change points of R factor time series and analyzed the relationships between rainfall erosivity and climate indices (such as the precipitation amount, number of effective events, and duration). Four trend tests such as the *t*-test, MK test, modified version of the MK test, and BBS-MK test, were used to detect trends in the annual R factor, total duration, number of effective events, total depth, mean maximum 30-min intensity, and total kinetic energy time series for all employed stations. The results provide insights into the evolution of rainfall erosivity and the effects of large-scale climatic circulation on rainfall erosivity.

1. Introduction

Soil erosion is a natural process in which the land surface is worn away by meteorological and geological agents, man-made land development, and other factors. Soil erosion has led to decreases in agricultural productivity by land degradation, increased landslide activity, ecosystem disturbances, and contaminant diffusion by the inflow of sediment yield to rivers. In South Korea, numerous researchers reported that soil erosion has been a major cause of the degradation of agricultural land and nonpoint pollution sources (Cho and Jeong, 2005; Kwon et al., 2002; Lee and Hwang, 2006).

In many countries, various efforts have been made to reduce soil loss and conserve soil and water quality. Some of these attempts involve the development of models for predicting the amount of soil loss or sediment yield such as; Universal Soil Loss Equation Model (Renard et al., 1997; Wischmeier and Smith, 1978), Water Erosion Prediction Project model (Haregeweyn et al., 2013), Water and Tillage Erosion Model/Sediment Delivery Model (Van Oost et al., 2000; Van Rompaey et al., 2001), the Agricultural Non-Point Source Pollution model (Haregeweyn and Yohannes, 2003), the Limburg Soil Erosion Model (Hengsdijk et al., 2005), Korean Soil Loss Estimation Model (Park, 2017) and so on. USLE (Universal Soil Loss Equation) and RUSLE (Revised Universal Soil Loss Equation) are well-known empirical models for estimating the long-term global average annual soil loss (Renard et al., 1997; Wischmeier and Smith, 1978). Over the last 40 years, the (R)USLE model has been widely used for predicting the average rate of soil erosion from arable land. Pandey et al. (2016) showed that 21 of 50 soil erosion and sediment yield models were adopted input parameters from the USLE model.

Rainfall erosivity is a numerical value that represents potential soil erosion by water and is the only climatic parameter of six factors in the (R)USLE model. It is defined as the long-term annual average of the

* Corresponding author at: Korea Military Academy, Dept. of Civil Engineering and Environmental Sciences, Hwarang-ro 564, Nowon-gu, Seoul 01805, South Korea.
E-mail address: cetera93@gmail.com (J.-H. Lee).

https://doi.org/10.1016/j.catena.2019.01.005
Received 15 July 2018; Received in revised form 4 January 2019; Accepted 8 January 2019
Available online 12 February 2019
0341-8162/

product of total rainfall energy (E) and the maximum 30-min rainfall intensity for individual storm events (Renard et al., 1997; Wischmeier and Smith, 1978).

Generally, the R factor value is bigger than the other parameters in (R)USLE and has greater annual spatial and temporal variations than the other indices except for the cover-management factor relatively; thus, spatial and temporal variations in soil loss are highly connected with variations in the R factor. Wischmeier (1959) reported that rainfall erosivity can explain approximately 80% of the variation in soil loss. Several researchers have emphasized that rainfall erosivity is extremely important input data for risk assessment for soil erosion (Aronica and Ferro, 1997; D'Odorico et al., 2001; Le Bissonnais et al., 2002). The rainfall erosivity values (the R factors) of many regions are expected to be altered due to the changes in rainfall patterns such as rainfall intensity and the frequency and spatial distribution of storm events that may occur with climate change. Recently, numerous researchers worldwide have reported the spatial and temporal variability of rainfall erosivity in study regions; for example, this variability was reported in Iran by Sadeghi et al. (2011); the Yangtze River Basin in China by Huang et al. (2013); a Himalayan watershed by Ma et al. (2014); Switzerland by Meusburger et al. (2012) and Schmidt et al. (2016); New Zealand by Klik et al. (2015); Southern Taiwan by Lee and Lin (2015); the Pearl River basin by Lai et al. (2016); the Central Rift Valley of Ethiopia by Meshesha et al. (2015); Colombia by Ávila and Ávila (2015); U.S. by Nearing (2001), and Biasutti and Seager (2015); Northern Algeria by Meddi et al. (2016); eastern African regions by Fenta et al. (2017); Europe by Ballabio et al. (2017); the Jaguari River basin in Brazil by Pontes et al. (2017); Italy by Borrelli et al. (2016); Hungary by Mezősi and Bata (2016); Greece by Panagos et al. (2016); Europe by Panagos et al. (2017); the Ganjiang River Catchment in China by Li and Ye (2018); and the Loess Plateau in China by Abd Elbasit et al. (2013) and Liu et al. (2018).

Rainfall erosivity is one of the most important factors in RUSLE, an empirical method to estimate the mean annual soil loss in certain areas. Thus, investigating spatial and temporal trends in rainfall erosivity is important for soil and water conservation planning. In South Korea, numerous studies about rainfall erosivity were conducted for the past 20 years, however, most of them were focused on the calculation of rainfall erosivity (Jung et al., 1983; Lee and Heo, 2011; Risal et al., 2016). On the other hand, some researchers have studied temporal variations in meteorological and hydrologic phenomena in response to climate change, particularly temperature and precipitation trends except for rainfall erosivity trends (Bae et al., 2008; Choi, 2004; Jung et al., 2002; Jung et al., 2011; Risal et al., 2016; Wang et al., 2006). Lee et al. (2018) analyzed rainfall erosivity variability using empirical orthogonal teleconnection (EOT) and empirical orthogonal function (EOF) decomposition techniques and investigated the impacts of climate on hydrologic variables in South Korea.

The purpose of this study is to investigate spatial and temporal variations in rainfall erosivity and erosivity density and to improve our understanding of the evolution of rainfall erosivity in South Korea, especially related to the rainfall events that have occurred since 2000. To determine the spatial variation in rainfall erosivity and erosivity density in South Korea, the spatial distributions of the R factor and erosivity density at monthly and annual time scales were drawn and analyzed. To investigate temporal variation in rainfall erosivity and erosivity density, trend detection tests were carried out for the monthly R factor and erosivity density. To find potential sources of R factor and erosivity density variation, trends in the time series of related variables, i.e., the precipitation amount, duration, maximum 30-min intensity and kinetic energy, the number of effective precipitation events and dependencies between the R factor and related variables, were examined. The results provide insights into the effects of large-scale climatic circulation on the evolution of rainfall erosivity and rainfall erosivity variability.

This paper is organized as follows. In Section 2, information and characteristics of the rainfall data are presented. In Section 3, a description of the employed methods, e.g., the trend test and interpolation scheme is presented. In Sections 4 and 5, the results of the spatial and temporal analyses are presented, respectively. Finally, the summary and conclusions are presented in Section 6.

2. Data

South Korea is located on the Korean Peninsula within the temperate climate region. The reported seasonality of precipitation in South Korea is very strong in the monsoon season. For instance, approximately 75% of the annual precipitation occurs from May to October. In addition, heavy rainfall events mainly occur in the rainy season. In the rainy season, two rainfall-generating mechanisms, i.e., local convective storms and typhoons, affect heavy rainfall events. The effects of monsoons in South Korea mainly cause local convective storm events. (Baek et al., 2017; Kang et al., 2005). Due to seasonal changes in atmospheric circulation, the East Asian summer monsoon is a major generating mechanism of heavy rainfall for approximately 3–4 weeks in the early rainy season (Im et al., 2008; Lau and Li, 1984). Typhoons cause very heavy rainfall events in the late rainy season (from late August to October) and provide approximately 25% of all seasonal precipitation (Baek et al., 2017; Kim and Jain, 2011). On average, three typhoons per year occur in South Korea (KMA, 2011).

In this study, 5-min precipitation data from 46 weather stations operated by the Korea Meteorological Administration (KMA) are adopted to investigate the characteristics of rainfall erosivity and erosivity density (rainfall erosivity per precipitation) in South Korea. The 5-min resolution is fine enough to obtain accurate maximum 30-min intensity data. The weather station locations are illustrated in Fig. 1 (a), and Table 1 presents information about the weather stations such as station name, record length, and elevation. The mean record length for all stations is approximately 45 years. This period is long enough to obtain reliable trend test results. From the beginning of the records to 1999, 5-min rainfall observations are available from April to October. The 5-min rainfall observations are available for all months from 2000 to 2015.

To examine the statistical characteristics of the annual precipitation time series of South Korea, basic statistics were calculated using the annual precipitation series for all of the stations and are presented in Table 1. To calculate annual precipitation data, the daily precipitation observations from the KMA database (data.kma.go.kr) were used. These basic statistics include the mean, standard deviation (SD), coefficient of variation (CV), coefficient of skewness (CS), and coefficient of kurtosis (CK). The mean of the annual precipitation means from all the employed stations is 1226 mm. The maximum and minimum annual precipitation means are 1664 mm and 950 mm, respectively. The annual precipitation means in South Korea have a high spatial variability. According to the CVs, the mean annual precipitation values of all stations, except for the Ulleungdo station, demonstrate a similar temporal variability. Since the Ulleungdo station is located on an island in the East Sea, its precipitation patterns may differ from those of the other stations. The CS and CK estimate means are 0.445 and 2.952, respectively. The CS and CK estimate means indicate the distribution of annual precipitation in South Korea follows a Gaussian distribution.

3. Methods

3.1. R factor calculation

The RUSLE R factor in Eq. (1) is used to obtain the annual and monthly R factor for the employed meteorological stations in South Korea. The R factor is a product of the kinetic energy (E) of a rainfall event and the maximum continuous 30-min intensity (I_{30}) within the rainfall event (Brown and Foster, 1987). The kinetic energy of a rainfall event is the sum of the products of estimated unit energy (e) and the

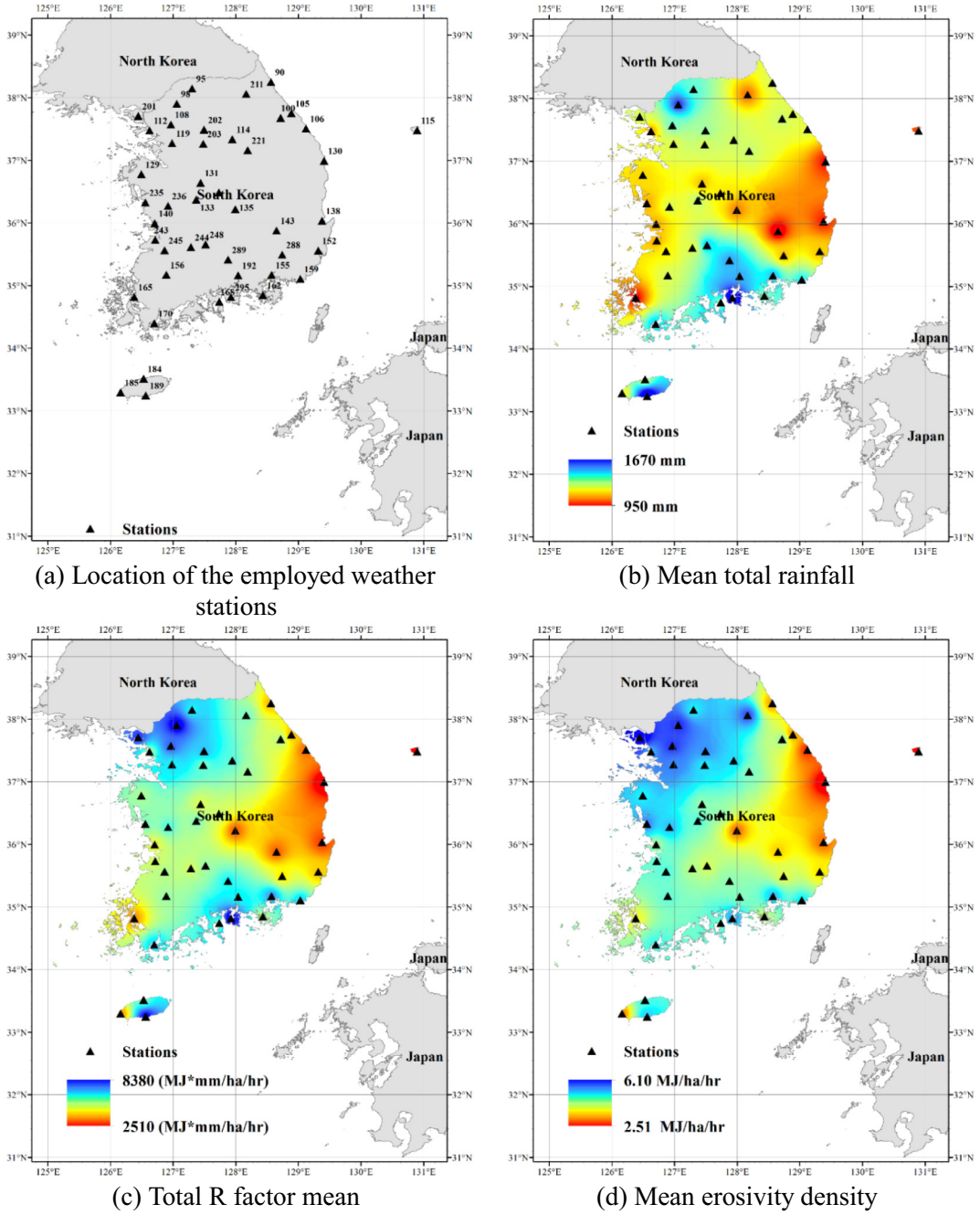

(a) Location of the employed weather stations (b) Mean total rainfall

(c) Total R factor mean (d) Mean erosivity density

Fig. 1. Location of the employed weather stations and spatial distribution of the mean total rainfall, total R factor mean, and mean erosivity density from April to October in South Korea.

depth of rainfall (ΔV) corresponding to the unit energy. The unit energy is computed using Eq. (2).

$$R_j = E_j \times I_{30,j} = \left(\sum_{r=1}^{n(j)} e_{r,j}\Delta V_{r,j}\right) \times I_{30,j} \quad (1)$$

$$e_{r,j} = 0.29[1 - 0.72\,exp(-0.05 i_{r,j})] \quad (2)$$

where E_j (MJ/ha), $I_{30,j}$ (mm/hr), $e_{r,j}$ (MJ/ha/mm), $\Delta V_{r,j}$ (mm), and $i_{r,j}$ (mm/hr) are the kinetic energy of the jth rainfall event, maximum 30-min rainfall intensity during the jth rainfall event, depth of rainfall for the rth period during the jth rainfall event, unit energy for the rth period during the jth rainfall event, and intensity for the rth period during the jth rainfall event, respectively. $n(j)$ is the number of period in the jth rainfall event.

An effective storm in (R)USLE is defined as the storm which causes to provoke soil erosion in effect. All storm events should be classified first using the criteria of Wischmeier and Smith (1978) to calculate the R factor; "Rain showers of less than 0.5 inch (12.5 mm) and separated from other rainfall periods by more than 6 hours were omitted from the rainfall erosivity computations, unless as much as 0.25 inch of rain fell in 15 minutes."

The effective storm events are selected from all individual rainfall events with a depth over 12.5 mm with more than 6.35.mm falling in 15 min (Foster et al., 2008). The 5-min precipitation data are used to calculate R factors for all individual rainfall events with the equations and criteria mentioned above. The R factor of a given month is the sum of the R factors of all individual rainfall events within that month. The R factor of a given year is the sum of all R factors within that year.

In South Korea, some regions have snowfalls from November to

Table 1
Information about the employed weather stations and basic statistics of annual rainfall for all employed stations (Note that SD, CV, CS, and CK indicate the standard deviation, coefficient of variation, coefficient of skewness, and coefficient of kurtosis, respectively).

Station code	Name	Recording period (the number of year)	Elevation (El.m)	Mean (mm)	SD (mm)	CV (%)	CS	CK
90	Sokcho	1968–2015 (48)	22.9	1216	292	24	0.737	3.078
95	Cheolwon	1988–2015 (28)	153.7	1321	322	24	0.140	2.324
98	Dongdocheon	1998–2015 (18)	109.1	1495	372	25	0.330	3.159
101	Chuncheon	1966–2015 (50)	772.4	1238	321	26	0.595	2.688
105	Gangneung	1961–2015 (55)	26.1	1212	317	26	1.191	4.163
106	Donghae	1992–2015 (24)	39.9	1210	375	31	0.346	2.198
108	Seoul	1961–2015 (55)	85.5	1311	360	27	0.674	2.845
112	Icheon	1961–2015 (55)	90.0	1109	283	26	0.614	2.864
114	Wonju	1973–2015 (43)	150.7	1236	307	25	0.729	3.614
115	Ulleungdo	1961–2015 (55)	220.0	1035	445	43	0.940	2.879
119	Suwon	1964–2015 (52)	34.5	1211	274	23	0.613	3.266
129	Seosan	1968–2015 (48)	25.2	1145	316	28	0.814	3.871
130	Uljin	1972–2015 (44)	49.4	1002	299	30	0.784	3.247
131	Cheongju	1967–2015 (49)	56.4	1126	273	24	0.452	2.406
133	Daejeon	1969–2015 (47)	62.6	1250	317	25	0.402	2.342
135	Chupungnyeong	1970–2015 (46)	240.9	1078	268	25	0.591	3.105
138	Pohang	1961–2015 (55)	1.3	1006	296	29	1.350	5.663
140	Gunsan	1968–2015 (48)	26.9	1110	311	28	0.286	2.281
143	Daegu	1961–2015 (55)	57.3	950	243	26	0.454	3.148
152	Ulsan	1961–2015 (55)	34.6	1134	307	27	0.559	2.466
155	Changwon	1985–2015 (31)	37.2	1390	374	27	−0.204	2.261
156	Gwangju	1961–2015 (55)	74.5	1221	338	28	−0.079	2.592
159	Busan	1961–2015 (55)	69.2	1349	402	30	0.534	2.505
162	Tongyeong	1968–2015 (48)	30.8	1305	345	26	0.408	3.029
165	Mokpo	1961–2015 (55)	37.4	991	295	30	0.157	2.360
168	Yoesu	1961–2015 (55)	73.3	1289	344	27	0.699	3.281
170	Wando	1972–2015 (44)	27.7	1377	405	29	0.273	2.365
184	Jeju	1961–2015 (55)	20.0	1253	395	32	0.848	3.590
185	Gosan	1998–2015 (18)	74.3	1183	267	23	−0.125	1.900
189	Seogwipo	1961–2015 (55)	50.4	1625	470	29	0.908	3.396
192	Jinju	1969–2015 (47)	27.1	1406	368	26	−0.188	2.091
201	Ganghwa	1973–2015 (43)	46.2	1225	328	27	1.039	4.531
202	Yangpyeong	1973–2015 (43)	47.4	1282	356	28	0.627	2.585
203	Icheon	1973–2015 (43)	90.0	1224	307	25	0.775	3.368
211	Inje	1973–2015 (43)	198.7	1066	354	33	−0.230	3.489
221	Jecheon	1973–2015 (43)	263.1	1240	370	30	0.522	3.089
226	Boeun	1973–2015 (43)	173.0	1162	346	30	0.809	3.308
235	Boryeong	1973–2015 (43)	17.9	1112	292	26	−0.092	2.518
236	Buyeo	1973–2015 (43)	11.0	1214	329	27	0.590	2.913
243	Buan	1973–2015 (43)	3.6	1112	311	28	0.633	4.296
244	Imsil	1973–2015 (43)	248.0	1204	320	27	0.031	2.589
245	Jeongeup	1973–2015 (43)	39.5	1173	301	26	0.302	2.680
248	Jangsu	1988–2015 (28)	406.5	1380	374	27	0.006	2.774
288	Miryang	1973–2015 (43)	10.7	1126	273	24	−0.181	2.192
289	Sancheong	1973–2015 (43)	138.7	1413	422	30	0.064	2.206
295	Namhae	1973–2015 (43)	43.2	1664	436	26	0.182	2.268
Mean				1226	335	27	0.455	2.952

March. The snow season of the stations depends on their locations. The precipitation record does not indicate whether an event is rainfall or snowfall. Rainfall in South Korea often occurs even when the air temperature, in degrees Celsius, is negative. Thus, it is impossible to perfectly classify snowfall or rainfall events from the precipitation data. Hence, in the current study, all recorded events are considered rainfall events in the winter season. Additionally, R factors are calculated from all individual precipitation events.

3.2. Erosivity density calculation

Erosivity density is a measure of the erosivity content per unit of precipitation. The erosivity density is the ratio of the monthly erosivity to monthly precipitation (Foster et al., 2008). Hence, the erosivity density is defined by Eq. (3).

$$\alpha_m = \frac{R_m}{P_m} \tag{3}$$

where α_m, P_m, and R_m are the monthly erosivity density (MJ/ha/h), monthly precipitation (mm), and monthly erosivity (MJ·mm/ha/h), respectively. To investigate the interannual variability in the erosivity density, the annual erosivity density is computed for the all employed stations. In the present study, the annual erosivity density is the ratio of annual rainfall erosivity to annual precipitation.

3.3. Spatial interpolation scheme

A number of spatial interpolation methods have been widely employed to spatially interpolate the R factor (Borrelli et al., 2016; Ferro et al., 2009; Panagos et al., 2015; Schmidt et al., 2016). Angulo-Martínez and Beguería (2009) and Hanel et al. (2016) reported the appropriateness of the regression-kriging approach in the spatial prediction of the R factor. To carry out the regression-kriging approach, covariates, such as monthly rainfall, annual rainfall, and minimum monthly rainfall, are used in regression modeling. Spatial observations or estimates of precipitation are required for the regression modeling. However, spatial observations or estimates are not available for precipitation in South Korea. Some global precipitation estimates, such as the WorldClim database (Fick and Hijmans, 2017), TRMM (Simpson et al., 1988), and CMORPH (Joyce et al., 2004), can be used for the

regression modeling. However, the precision of monthly precipitation estimates from the WorldClim database has not been evaluated for the precipitation in South Korea. In addition, a bias-correction procedure must be applied to satellite global precipitation products for spatial interpolation because their precision is not good enough for direct use (Kim et al., 2016). Due to lack of the spatial observations of precipitation in South Korea, the regression-kriging approach cannot be used to determine the R factor of South Korea. Beguería et al. (2018) proposed a method for computing rainfall erosivity using the daily precipitation amount, and this method can provide high temporal and spatial resolution R factor data. In the current study, this method is not applied to spatially interpolated R factors since the spatial characteristics of precipitation and erosivity density are also examined.

In the current study, the inverse distance weight (IDW) method is used for the spatial interpolation scheme. The IDW method is carried out with the underlying assumption that an attribute value at an unobserved location is the weighted average of known data points from local neighboring region surrounding the unobserved location. The IDW method can calculate the R factor of an unobserved location without the use of external variables, except for location information. This method is appropriate for spatially interpolating R factor data in South Korea. In addition, the IDW method has been adapted as an interpolation scheme for the R factor by Millward and Mersey (1999), Xin et al. (2010), Huang et al. (2013), Risal et al. (2016), and Sadeghi et al. (2017). In the current study, the spatial interpolation of the R factor is performed in ESRI ArcGIS using the IDW method.

3.4. Trend detection tests

Parametric and nonparametric tests have been widely employed to detect time series trends. Because each method has pros and cons, several trend detection tests must be employed for accurate trend detection. In the current study, the *t*-test for trend detection is employed as a parametric trend test. MK is employed as a nonparametric test. The results of the MK trend test are affected by serial correlation in the time series, i.e., when positive serial correlation exists within a time series, the results of the MK test may be worse (von Storch, 1999; Yue et al., 2002). Completely independent datasets are difficult to find due to the presence of external factors that influence data. To overcome these drawbacks, a high number of studies have suggested the use of various modified versions of the MK test in the field of hydrometeorology (Hamed and Rao, 1998; Önöz and Bayazit, 2012; Yue and Wang, 2004; Yue and Wang, 2002a). In the present study, a modified version of the MK test and block bootstrap-based MK tests are also employed as trend detection tests in order to improve the trend detection test results.

3.4.1. t-test

In the t-test for trend detection, the significance of the slope parameter in a linear regression model is tested based on the t-distribution. The null hypothesis of the *t*-test is that there is no trend in the data. If the test statistic is greater or smaller than the given thresholds, i.e., the significance level, the null hypothesis is rejected. In the present study, the simple linear regression model is given by Eq. (4).

$$R_i = a \bullet i + b \tag{4}$$

where R_i, a, and b are *i*th rainfall erosivity, slope, and offset, respectively. The *t*-test statistic (τ) corresponding to the slope estimate ($\hat{a}$) can be obtained by Eq. (5).

$$\tau = \frac{\hat{a}\sqrt{n-2}}{\sqrt{\frac{\sum_i^n (R_i - \overline{R_i})^2}{\sum_i^n (i - \bar{i})^2}}} \tag{5}$$

where n, $\overline{R_i}$, and $\bar{i}$ are the number of data points, mean of R_i and mean of *i*, respectively. τ follows the t-distribution with n-2 degrees of freedom. In the current study, the 5% significance level is employed in the t-test.

3.4.2. Mann-Kendall test

The test statistic (*S*) used in the MK test is given as follows:

$$S = \sum_{i=1}^{n-1} \sum_{j=i+1}^{n} sign(Y_j - Y_i), \qquad sign(\alpha) = \begin{cases} 1 \; if \; \alpha > 0 \\ 0 \; if \; \alpha = 0 \\ -1 \; if \; \alpha < 0 \end{cases} \tag{6}$$

where Y_i and Y_j are the sequential data values, and n is the total number of observations in the time series. A positive value of the test statistic *S* indicates an increasing trend, whereas a negative value of this quantity indicates a decreasing trend. Mann (1945) and Kendall (1948) report that when n is larger than eight, the statistic S is approximately normally distributed with the variance given by the following:

$$\mathrm{V(S)} = \frac{n(n-1)(2n+5) - \sum_{l=1}^{n} t_l l(l-1)(2l+5)}{18} \tag{7}$$

where t_l is the number of ties of extent l. The standard MK statistic Z is computed by Eq. (8)

$$\mathrm{Z} = \begin{cases} \dfrac{S-1}{\sqrt{V(S)}} & for \; S > 0 \\ 0 \quad for \; S = 0 \\ \dfrac{S+1}{\sqrt{V(S)}} & for \; S < 0 \end{cases} \tag{8}$$

The standard MK statistic Z follows the standard normal distribution under the null hypothesis of no trend. In the current study, a 5% significance level is employed in the MK test.

3.4.3. Modified version of the Mann-Kendall test

It is difficult to appropriately detect a trend in data with a serial correlation and small sample size. To obtain reliable trend detection results, a modified version of the MK test adapted by Yue and Wang (2002b) is employed in the current study. In the modified MK test, the autocorrelation in the data series is taken into account by modifying the test statistics variance. The modified MK test procedure is described below.

In the modified MK test, the variance of the test statistics V(S) is corrected by multiplication with a correction factor (CF) used to address the serial correlation in the data. Eq. (9) presents the corrected test statistics variance.

$$\mathrm{V^*}(S) = CF * V(S) \tag{9}$$

$$CF = \begin{cases} 1 + 2\dfrac{\rho_1^{n+1} - n\rho_1^2 + (n-1)\rho_1}{n(\rho_1 - 1)^2} & for \; i = 1 \\ 1 + 2 * \sum_{i=1}^{n-1} \left(1 - \dfrac{i}{n}\right)\rho_i & for \; i > 1 \end{cases} \tag{10}$$

where ρ_i is the lag-*i* serial correlation coefficient from the detrended data or the rank of the detrended data. In the current study, the trends in the original data are removed by the Theil-Sen approach, as recommend by Hamed and Rao (1998). Eq. (10) was given by Matalas and Langbein (1962) and Bayley and Hammersley (1946). The standard Mk statistic Z^* in the modified MK test is defined by Eq. (11).

$$\mathrm{Z^*} = \begin{cases} \dfrac{S-1}{\sqrt{V(S)^*}} & for \; S > 0 \\ 0 \quad for \; S = 0 \\ \dfrac{S+1}{\sqrt{V(S)^*}} & for \; S < 0 \end{cases} \tag{11}$$

In the current study, a 5% significance level is employed in the modified version of the MK test.

3.4.4. Block bootstrap-based Mann-Kendall test

The block bootstrap-based MK (BBS-MK) test, which is a modified

version of the MK test, was described by Khaliq et al. (2009). The performance of the BBS-MK test is comparable to that of other modified versions of the MK test, but it is simpler and more efficient than other methods (Önöz and Bayazit, 2012). The procedure used for applying the BBS-MK test is as follows:

1) Estimate the statistic S of the MK test from the original time series.
2) Estimate the number of significant contiguous autocorrelations, k. When the autocorrelation is smaller than the 5% significance level, the lag of the autocorrelation becomes k.
3) Estimate optimum value of g. To find the optimum g value, the mean and autocorrelation of the observed and resampled data are computed. The relative absolute error between the observed and resampled data for g from one to 1/4 of the sample size is computed based on the mean and autocorrelation estimates. The g value giving the smallest relative error is employed as the optimum value. The block size of the BBK-MK test is defined by k + g.
4) Resample the original time series a large number of times using the estimated block size.
5) Estimate the test statistic S for each simulated sample to produce a simulated distribution of the test statistic S.
6) Estimate the significance (*p*-value) of the test statistic *S* estimated in step 1 using the simulated distribution from step 5.

In this study, 2000 simulated sample sets are resampled from the original dataset. Svensson et al. (2005) showed that 2000 realizations can provide stable estimates of significance in trend tests using simulation methods. A detailed method for finding optimum values of g was described in Khaliq et al. (2009) and Önöz and Bayazit (2012). In the current study, a 5% significance level is employed in the BBS-MK test.

4. Spatial distributions of precipitation, rainfall erosivity and erosivity density

4.1. Spatial distributions of the annual precipitation, the annual rainfall erosivity, and the annual erosivity density

Annual R factors for each station needed to be calculated to investigate the spatial distribution of R factors in South Korea. We computed annual R factors using 5-min precipitation data, which were available from March to November (9 months) before 2000 and from January to December (12 months) from 2000 to 2015. The total R factor from April to October is almost 95% of the annual R factor in South Korea (see Table A2). The proportion of the total R factor from April to October to the annual R factor could be larger than 95% due to snowfall events from November to March. The spatial distribution characteristics of the total R factor from April to October and the annual R factor are similar. The use of a large number of data points in estimating fundamental R factor characteristics leads to more reliable results (Foster et al., 2008). Thus, in the current study, the total R factors from April to October are employed as annual R factors for examining of the spatial distribution of the annual R factor. The erosivity density from April to October represents the total R factor over the total precipitation amount.

Table 2 presents the total rainfall erosivity (R factor) from April to October and the associated basic statistics for all employed stations. The mean of the R factor means for all stations is 5349 MJ·mm/ha/h/yr, while the R factor ranges from 2512 MJ·mm/ha/h/yr to 8379 MJ·mm/ha/h/yr for all stations. In South Korea, the maximum R factor is more than three times the minimum rainfall erosivity. The SD and CV means are 2867 MJ·mm/ha/h/yr and 54%, respectively. Based on the CV values, the interannual variability in the R factor is greater than the annual precipitation variability shown in Table 1. The CS mean for the total R factor from April to October is 1.258. The total R factors of many stations in South Korea may have nonnormal distributions such as exponential and gamma distributions. Additionally, large CSs are observed in a number of stations in coastal regions. CSs of eleven stations within all stations are larger than 1.5. Eight of them are located at coastal regions. Lengths of the series for the eight stations are longer than have thirty-one. Twenty-four stations have CSs larger than 1.0. The fourteen stations of them are located in coastal regions. The five largest CSs were observed at the stations in coastal regions. Lengths of the series for the eight stations are longer than have twenty-eight. The mean CK of the total R factor is higher than the mean CK of the annual precipitation.

Table 2
Basic statistics of rainfall erosivity (R factor) from April to October for all employed stations (Note that SD, CV, CS, and CK represent the standard deviation, coefficient of variation, coefficient of skewness, and coefficient of kurtosis, respectively).

Station code	Name	Mean (MJ mm/ha/h/yr)	SD (MJ mm/ha/h/yr)	CV (%)	CS	CK
90	Sokcho	4015	2301	57	2.279	9.657
95	Cheolwon	6206	2686	43	0.286	2.123
98	Dongdocheon	8224	4843	59	0.940	3.079
101	Chuncheon	5337	2603	49	0.558	2.651
105	Gangneung	3962	3050	77	3.645	19.942
106	Donghae	3379	2058	61	1.438	4.533
108	Seoul	7186	4127	57	1.239	4.763
112	Icheon	5489	3008	55	0.840	2.809
114	Wonju	5914	2468	42	0.880	3.663
115	Ulleungdo	2646	1505	57	1.458	5.130
119	Suwon	6206	2927	47	1.099	3.719
129	Seosan	5381	3380	63	1.804	7.157
130	Uljin	2512	1125	45	0.427	2.280
131	Cheongju	4884	2117	43	0.558	2.644
133	Daejeon	5661	2881	51	0.962	3.602
135	Chupungnyeong	3288	1291	39	0.540	2.490
138	Pohang	3075	2551	83	5.079	32.855
140	Gunsan	4695	2442	52	1.078	3.451
143	Daegu	3311	1411	43	0.423	2.471
152	Ulsan	4101	2353	57	1.255	4.301
155	Changwon	6810	5555	82	3.361	16.024
156	Gwangju	5486	2579	47	0.694	3.324
159	Busan	6341	3426	54	0.783	2.722
162	Tongyeong	5311	2806	53	1.900	9.170
165	Mokpo	3701	1910	52	1.938	8.717
168	Yoesu	5686	2447	43	0.992	4.484
170	Wando	6347	3052	48	0.824	3.231
184	Jeju	5742	3674	64	1.181	3.739
185	Gosan	3740	1613	43	0.164	2.034
189	Seogwipo	7893	4002	51	1.404	4.926
192	Jinju	6160	2783	45	0.500	3.250
201	Ganghwa	7469	5220	70	2.541	10.879
202	Yangpyeong	6521	3624	56	1.005	3.504
203	Icheon	5765	2998	52	1.293	4.746
211	Inje	5725	3316	58	1.690	6.360
221	Jecheon	5455	2832	52	0.680	3.114
226	Boeun	5034	3262	65	2.270	8.516
235	Boryeong	5707	3301	58	1.145	4.236
236	Buyeo	5958	3866	65	1.727	6.053
243	Buan	5006	2267	45	1.279	5.727
244	Imsil	5007	2226	44	0.422	2.282
245	Jeongeup	5334	2892	54	1.268	3.937
248	Jangsu	5492	2289	42	0.416	2.370
288	Miryang	4371	2057	47	0.527	2.397
289	Sancheong	6147	3181	52	0.422	2.197
295	Namhae	8379	3574	43	0.640	2.829
Mean		5349	2867	54	1.258	5.524

Table 3 presents the means of the erosivity densities from April to October and the associated basic statistics for all employed stations. The mean of the erosivity density means from April to October is 4.14 MJ/ha/h, and the erosivity density means of all stations range from 2.4 MJ/ha/h to 5.8 MJ/ha/h. The SD and the CV of the erosivity density means from April to October are 1.454 MJ/ha/h and 35%, respectively. The erosivity density interannual variability is larger than the annual precipitation variability but smaller than the R factor variability. The CS

Table 3
Basic statistics of erosivity density from April to October for all employed stations (Note that SD, CV, CS, and CK represent the standard deviation, coefficient of variation, coefficient of skewness, and coefficient of kurtosis, respectively).

Station code	Name	Mean (MJ/ha/h)	SD (MJ/ha/h)	CV (%)	CS	CK
90	Sokcho	3.23	1.35	42	1.80	7.40
95	Cheolwon	4.55	1.23	27	−0.14	2.22
98	Dongdocheon	5.17	1.97	38	0.41	2.08
101	Chuncheon	4.13	1.33	32	0.21	2.26
105	Gangneung	3.10	1.44	47	2.11	9.47
106	Donghae	2.73	1.22	45	1.41	4.11
108	Seoul	5.16	1.77	34	0.55	3.43
112	Icheon	4.72	1.83	39	0.82	3.50
114	Wonju	4.69	1.31	28	1.03	4.86
115	Ulleungdo	2.55	0.88	35	0.86	3.36
119	Suwon	4.97	1.56	31	0.85	3.61
129	Seosan	4.45	1.83	41	1.41	6.00
130	Uljin	2.43	0.64	26	0.47	3.42
131	Cheongju	4.25	1.32	31	0.36	3.62
133	Daejeon	4.37	1.49	34	0.45	2.57
135	Chupungnyeong	3.02	0.86	28	0.79	3.85
138	Pohang	2.91	1.32	45	4.10	24.77
140	Gunsan	4.07	1.22	30	0.53	3.06
143	Daegu	3.41	1.04	31	0.90	4.02
152	Ulsan	3.46	1.34	39	0.85	3.02
155	Changwon	4.61	2.61	57	3.28	15.42
156	Gwangju	4.34	1.26	29	0.79	3.88
159	Busan	4.51	1.67	37	1.02	3.97
162	Tongyeong	3.93	1.35	34	1.03	4.26
165	Mokpo	3.65	1.15	32	1.53	6.95
168	Yoesu	4.30	1.03	24	0.05	2.70
170	Wando	4.51	1.53	34	1.67	6.56
184	Jeju	4.31	1.83	43	0.98	3.39
185	Gosan	3.08	0.96	31	−0.01	1.76
189	Seogwipo	4.71	1.40	30	1.03	4.11
192	Jinju	4.23	1.19	28	0.67	4.85
201	Ganghwa	5.82	2.83	49	2.01	7.77
202	Yangpyeong	4.83	1.64	34	0.42	2.37
203	Icheon	4.54	1.56	34	0.68	2.97
211	Inje	4.40	1.52	35	0.93	3.02
221	Jecheon	4.19	1.34	32	0.27	2.80
226	Boeun	4.14	1.58	38	1.59	6.51
235	Boryeong	4.88	1.95	40	1.09	5.32
236	Buyeo	4.66	2.03	44	1.53	5.46
243	Buan	4.47	1.47	33	0.78	2.94
244	Imsil	4.03	1.04	26	−0.12	2.97
245	Jeongeup	4.41	1.67	38	1.32	4.79
248	Jangsu	3.91	1.01	26	0.00	3.19
288	Miryang	3.76	1.24	33	0.55	2.30
289	Sancheong	4.14	1.39	34	0.66	3.72
295	Namhae	4.93	1.38	28	1.23	5.28
Mean		4.14	1.45	35	0.97	4.78

and the CK of the erosivity density means are 1.258 and 5.524, respectively. Based on the CS, the mean erosivity density distributions seem to be slightly skewed. The distribution of the mean erosivity density for some stations may be nonnormal.

Fig. 1 (b) to (d) presents the spatial distribution of the mean annual precipitation, the total rainfall erosivity (R factor) mean, and the erosivity density mean from April to October in South Korea. In Fig. 1 (b), large amounts of the total precipitation are observed in the southern and northwestern regions. Small amounts of the total precipitation are observed in the southeastern and western regions. The southeastern region of South Korea is drier than other regions and frequently experiences drought in the winter and spring seasons. Overall, the spatial pattern of the total R factor means in Fig. 1 (c) is similar to the spatial pattern of annual precipitation. The total R factors in the western region show intermediate values, unlike precipitation in the same region. Additionally, the eastern coastal region has small total R factor mean values. The stations in the northwestern region have large total R factor mean values compared to stations in other regions.

Table 4
Basic statistics of monthly rainfall, rainfall erosivity, and erosivity density in South Korea.

Variables	Statistics	Apr.	May	Jun.	Jul.	Aug.	Sep.	Oct.
Rainfall (mm)	Mean	98	108	162	293	271	156	60
	Proportion (%)	8.6	9.4	14.1	25.5	23.6	13.6	5.2
	SD	58	63	105	158	162	123	51
	CV (%)	59	58	65	54	60	79	85
	CS	0.91	0.87	1.19	0.96	1.03	1.1	1.43
	CK	3.84	4.37	4.71	4.12	4.14	4.14	5.58
Rainfall erosivity (R factor) (MJ·mm/ha/h/yr)	Mean	182	270	592	1702	1705	726	171
	Proportion (%)	3.4	5	11.1	31.8	31.9	13.6	3.2
	SD	233	345	683	1540	1764	1022	353
	CV (%)	128	128	115	90	103	141	206
	CS	2.53	2.21	2.18	1.79	2	2.33	3.32
	CK	11.62	9.23	9.04	7.12	8.03	9.58	16.83
Erosivity density (MJ/ha/h)	Mean	1.34	1.85	2.89	5.01	5.25	3.5	1.86
	Proportion (%)	6.2	8.5	13.3	23.1	24.2	16.1	8.6
	SD	1.03	1.34	1.92	2.63	2.89	3.67	3.36
	CV (%)	76	73	67	52	55	105	181
	CS	1.6	1.46	1.1	1.15	1.07	1.48	2.88
	CK	7.7	6.44	5.01	5.55	4.66	6.83	15.6

The spatial pattern of the mean erosivity density is more similar to the spatial pattern of the mean total R factor than that of the mean total precipitation. Large erosivity densities are observed in the northwestern region. Overall, the precipitation, R factor, and erosivity density spatial distribution patterns are similar to each other. Since R factor and erosivity density values are related to the magnitude of precipitation events, a large amount of precipitation leads to large R factor and erosivity density values, and vice versa.

4.2. Spatial distributions of the monthly precipitation, the monthly rainfall erosivity, and the monthly erosivity density

To investigate the seasonal variability in the precipitation, rainfall erosivity, and erosivity density spatial distribution, the monthly R factor and monthly erosivity density means are computed. The 5-min rainfall data are available for the entire year from 2000 to 2015. Thus, monthly R factors are computed from April to October. Basic monthly rainfall, monthly R factor, and monthly erosivity density statistics are presented in Table 4. The monthly precipitation means range from 29 mm to 293 mm. The minimum and maximum monthly R factor mean values are 21 MJ·mm/ha/h and 1705 MJ·mm/ha/h, respectively. The monthly erosivity density means range from 0.4 MJ/ha/h to 5.25 MJ/ha/h.

> 75% of the annual precipitation, 95% of the total annual R factor and 85% of total erosivity density occurs from April to October. These results indicate a very large R factor seasonal variability. According to Table 4, the seasonal variability of the erosivity density is larger than that of precipitation but smaller than that of the R factor. The precipitation, R factor, and erosivity density CVs for each month can represent the interannual variability of these factors in each month. Overall, the R factor CVs are larger than the precipitation and erosivity density CVs. From the result, it can be inferred that the monthly R factor may drastically change from year to year. This high interannual variability of monthly R factor is the most probably occurred by extreme precipitation events in each year since the R factor is highly correlated to magnitude and intensity of the precipitation event. The largest monthly precipitation, monthly R factor, and monthly erosivity density CVs are observed in October. One or no typhoons pass through South Korea in October (KMA, 2011). Thus, the high CV variability in October may be caused by the influence of typhoons.

The spatial distributions of mean monthly precipitation, rainfall erosivity, and erosivity density are presented in Figs. 2 to 4,

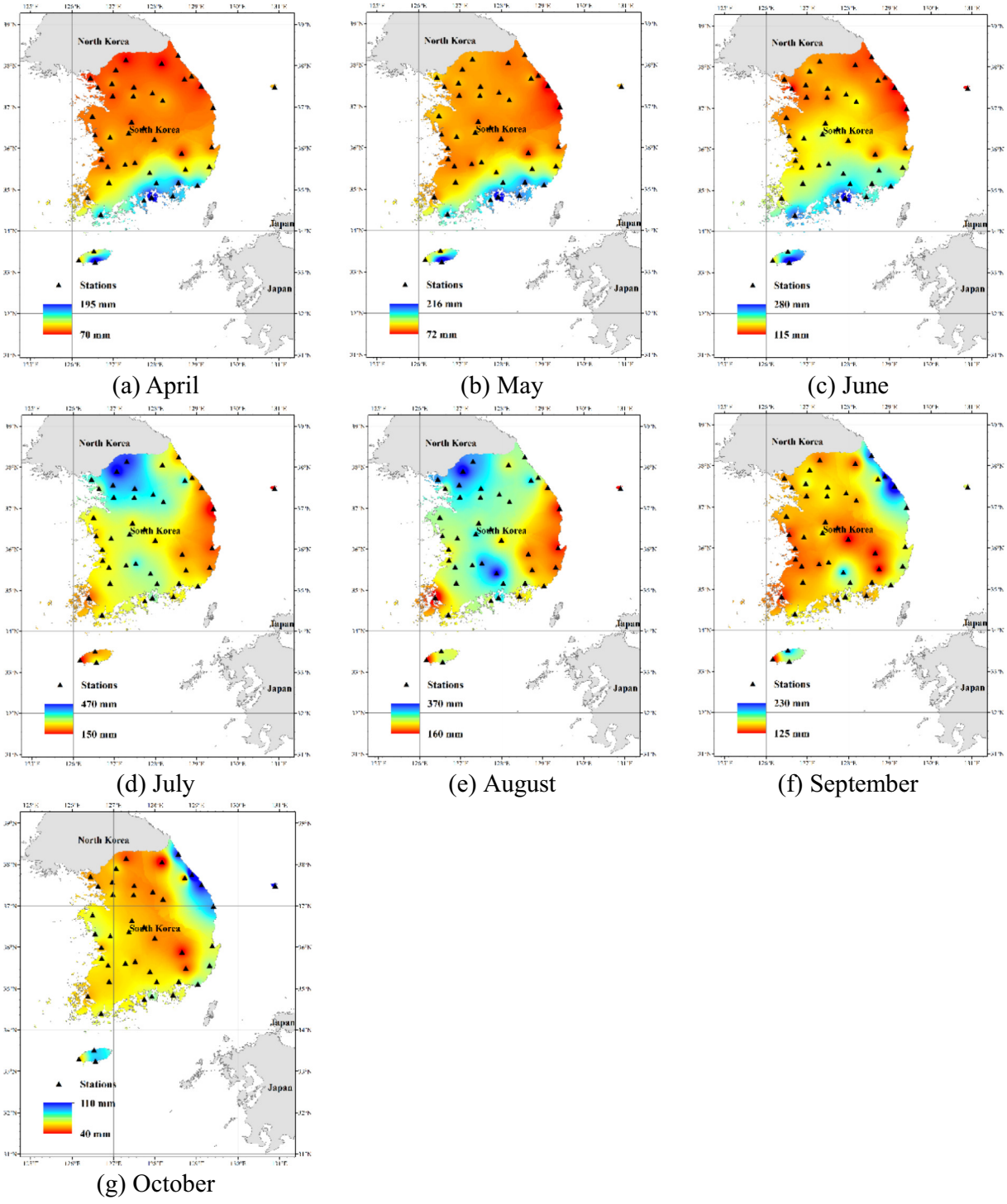

Fig. 2. Spatial distributions of the mean monthly precipitation in South Korea.

respectively. For the monthly precipitation, larger values are observed in the coastal region than those of inland regions for all months except for July and August while large amount of precipitation are observed in northern and southern regions for July and August. Large amounts of precipitation are observed in the southern coastal region from February to June and in the eastern coastal region from September to October. Fig. 2 shows that the seasonal change in the spatial distribution of monthly precipitation is large.

Unlike the case of the total precipitation and the total R factor mean from April to October, the spatial distributions of the monthly mean R factors are dissimilar from those of the monthly precipitation. From April to May, the monthly R factor means of the stations located in the southern coastal region show relatively high values. The R factor spatial distributions in July and August govern the annual R factor spatial distribution. The seasonal variability in the monthly mean R factor spatial distributions and the R factor spatial variability for each month are very high.

The mean monthly erosivity density and monthly R factor spatial distributions are similar. The largest difference between the mean monthly R factor and erosivity density spatial distribution is observed on June. In Fig. 4 (f), the monthly erosivity density means in the western region are relatively uniform compared to the monthly R factor

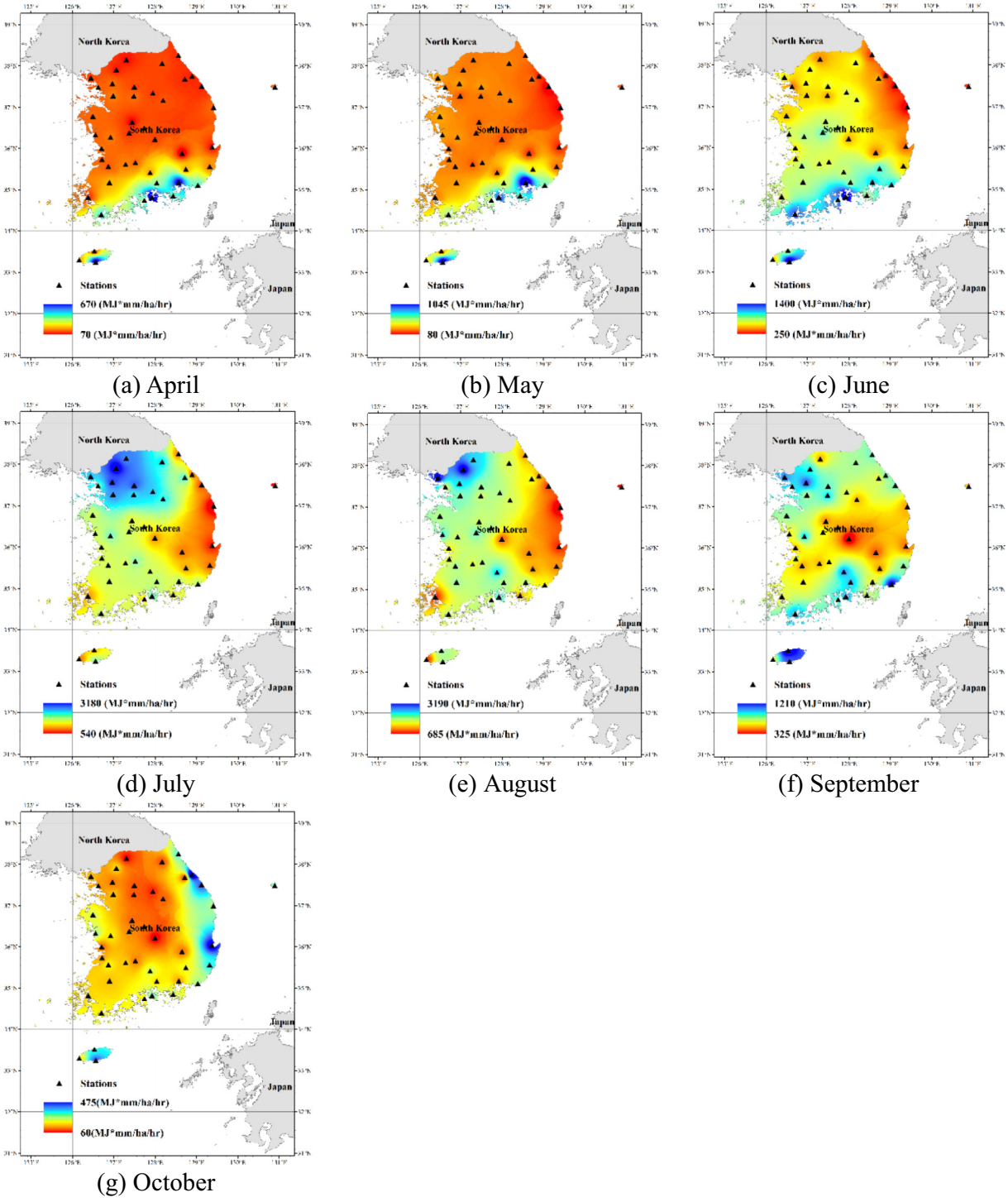

Fig. 3. Spatial distributions of the mean monthly rainfall erosivity in South Korea.

mean spatial distributions in the same regions. In June and July, the East Asian summer monsoon, known as Changma in South Korea, is the main generating mechanism of rainfall events (Lee and Seo, 2013). The Changma is a large-scale rainfall event compared to territory size of South Korea. Since the Changma provides precipitation to a very wide area, the spatial variability in the monthly erosivity density means from June to July may be low, and the spatial distribution of mean erosivity density in the two months may be similar.

5. Trends in the time series of rainfall erosivity and erosivity density

5.1. Trends in the time series of the annual rainfall erosivity

The trend in the rainfall erosivity (R factor) time series from April to October was determined by the four described trend detection tests. Furthermore, trends in the time series of R factor-associated variables, i.e., the mean number of effective events, duration, depth, intensity, and kinetic energy, were determined from April to October to investigate which variables affect temporal changes in the rainfall

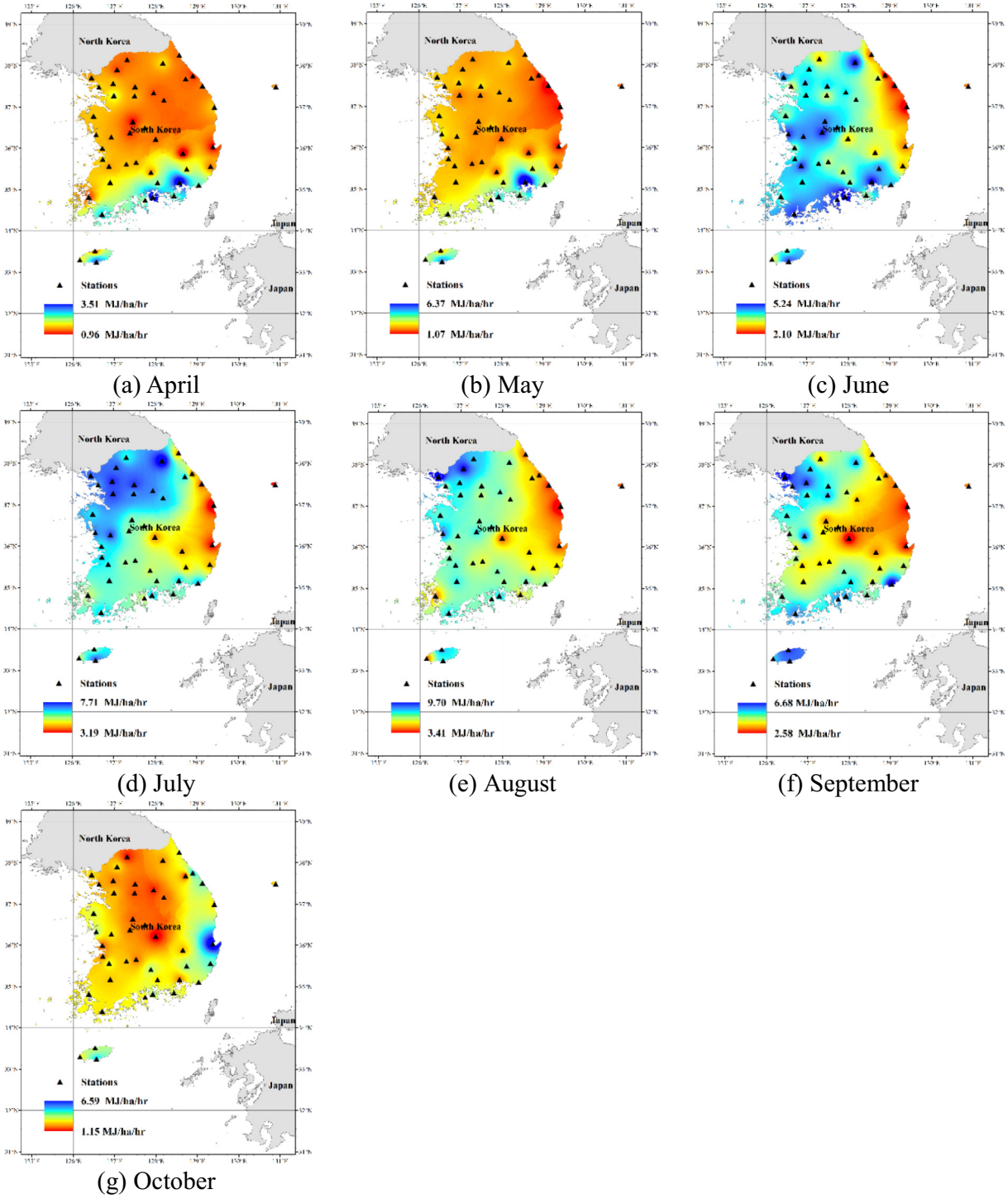

Fig. 4. Spatial distributions of the mean monthly erosivity density in South Korea.

erosivity time series. The number of effective rainfall events was used in the R factor computation. The total duration, depth, mean maximum 30-min intensity, and total kinetic energy of all effective events in each year represent the characteristics of effective rainfall events.

Table 5 presents the results of the four trend tests for all employed stations. Significant increasing trends were detected in the R factor time series of five stations (#98, #115, #156, #189, and #244). This result indicates that the R factor time series in South Korea may not exhibit a trend. Jung et al. (2017) investigated temporal variability in extreme precipitation in South Korea and found that precipitation events in South Korea overall show no significant trends. Extreme precipitation events, particularly those in South Korea, largely affect R factor values because a few intensive rainfall events dominate the annual R factor magnitude. Therefore, the trend test results for the R factor are reasonable.

The time series of the number of effective events at station #221 demonstrated a significant increasing trend. However, the R factor time series for station #221 has no significant trend. In fifteen stations, based on the results of the employed trend tests, the duration time series have significant trends; however, these trends demonstrate no consistent sign. The total rainfall depth time series of nine stations have significant trends. At four stations (#115, #156, #189, and #224), 80% of the

Table 5
Trend detection results for the annual R factors and R factor-related variables of all employed stations (Note that bold indicates stations with a significant trend detected by any trend detection test in the R factor series. The numbers indicate how many tests detected a trend in the times series for the variable of interest. Positive and negative signs indicate increasing and decreasing trends, respectively. The numbers in bracket are trend detection test results for same periods, i.e. from 1986 to 2018.).

Station code	R factor	The number of effective events	Total duration	Total rainfall depth	Max intensity mean	Total kinetic energy
90	0(0)	0(0)	−1(−3)	0(3)	0(0)	0(0)
95	0(−)	0(−)	0(−)	0(−)	0(−)	0(−)
98	**2(−)**	**0(−)**	**0(−)**	**0(−)**	**0(−)**	**0(−)**
101	0(0)	0(0)	−4(0)	0(0)	0(0)	0(0)
105	0(0)	0(0)	0(4)	0(4)	3(0)	0(0)
106	0(−)	0(−)	0(−)	0(−)	0(−)	0(−)
108	0(0)	0(0)	−3(0)	0(0)	0(0)	0(0)
112	0(0)	0(0)	−3(0)	0(0)	0(0)	0(0)
114	0(0)	0(0)	0(1)	0(1)	0(0)	0(0)
115	**4(4)**	**0(0)**	**0(0)**	**3(0)**	**4(0)**	**4(3)**
119	0(0)	0(0)	−4(0)	0(0)	0(0)	0(0)
129	0(0)	0(0)	0(0)	0(0)	0(0)	0(0)
130	0(0)	0(0)	0(0)	0(0)	0(0)	0(0)
131	0(0)	0(0)	0(0)	0(0)	0(0)	0(0)
133	0(0)	0(0)	−3(0)	0(0)	0(0)	0(0)
135	0(0)	0(0)	0(0)	0(0)	0(0)	0(0)
138	0(0)	0(0)	0(0)	0(0)	0(2)	0(0)
140	0(0)	0(0)	0(0)	0(0)	0(0)	0(0)
143	0(0)	0(0)	−4(0)	0(0)	3(4)	0(0)
152	0(0)	0(0)	0(0)	0(0)	0(0)	0(0)
155	0(0)	0(0)	0(0)	0(0)	0(0)	0(0)
156	**3(3)**	**0(0)**	**−3(0)**	**3(0)**	**4(0)**	**0(0)**
159	0(0)	0(0)	−4(−4)	0(4)	3(4)	0(0)
162	0(0)	0(0)	0(0)	0(0)	2(3)	0(0)
165	0(0)	0(0)	0(0)	2(0)	4(0)	0(0)
168	0(0)	0(0)	0(0)	4(0)	4(0)	0(0)
170	0(0)	0(0)	0(0)	0(0)	0(0)	0(0)
184	0(0)	0(0)	−2(−4)	0(4)	0(0)	0(0)
185	0(−)	0(−)	0(−)	0(−)	0(−)	0(−)
189	**3(3)**	**0(0)**	**0(1)**	**3(1)**	**4(0)**	**4(1)**
192	0(0)	0(0)	−4(0)	0(0)	0(0)	0(0)
201	0(0)	0(0)	0(0)	0(0)	0(0)	0(0)
202	0(0)	0(0)	3(0)	3(0)	0(0)	3(1)
203	0(0)	0(0)	3(0)	0(0)	0(0)	0(0)
212	0(0)	0(0)	0(0)	2(0)	0(0)	0(0)
221	0(0)	3(0)	4(0)	4(0)	3(0)	0(0)
226	0(0)	0(0)	0(0)	0(0)	0(0)	0(0)
235	0(0)	0(0)	0(0)	0(0)	0(0)	0(0)
236	0(0)	0(0)	3(0)	0(0)	0(0)	0(0)
243	0(0)	0(0)	0(0)	0(0)	0(0)	0(0)
244	**1(1)**	**0(0)**	**0(0)**	**2(0)**	**0(0)**	**0(0)**
245	0(−)	0(−)	0(−)	0(−)	0(−)	0(−)
248	0(0)	0(0)	0(0)	0(0)	0(0)	0(0)
288	0(0)	0(0)	0(0)	0(0)	0(0)	0(0)
289	0(0)	0(0)	0(0)	0(0)	4(0)	0(0)
295	0(0)	0(0)	0(0)	0(0)	0(0)	0(0)

stations showing a significant R factor trend, also had significant trends for total rainfall depth. Based on the trend test results, total rainfall depth may influence R factor time series trends. Significant trends, which are all increasing, are detected in the maximum 30-min intensity time series of eleven stations. Stations #115, #156 and #189 demonstrate significant R factor and maximum 30-min intensity time series trends. Based on the trend tests results, the total kinetic energy time series of three stations (#115, #189, and #202) have positive significant trends. Notably, at stations with significant trends in total kinetic energy the total rainfall depth time series also demonstrate significant trends. However, the total kinetic energy time series are not significant when there are significant trends in the total rainfall depth. For stations #115 and #189, significant trends are detected in the R factor and the total kinetic energy time series.

To further examine the relations among R the factor and R factor-associated variables and to determine the influence of these associated variables, Pearson correlations between the R factor and the variables were computed. The mean correlation matrix values for all stations are presented in Table 6. R factor has strong correlations with the total rainfall depth; mean maximum 30-min intensity, and total kinetic energy and low correlations with the number of effective events and the total duration variables. This result indicates that all variables affect the R factor value. The kinetic energy and the maximum 30-min intensity may have high correlations with the R factor because they are used when calculating the R factor. Among all variables, the total kinetic energy has the strongest correlation with the R factor. The total rainfall depth and mean maximum 30-min intensity demonstrate the second and third strongest correlations, respectively, with the R factor. Based on the correlation matrix results, R factor time series trends may be mainly influenced by trends in the kinetic energy time series. However, based on the trend test results shown in Table 5, maximum 30-min intensity time series trends may have a stronger influence than total kinetic energy time series trends on R factor trends in South Korea.

Based on the correlations among the variables, the total kinetic energy has strong correlations with all variables except for the mean maximum 30-min intensity. Since the number of effective events, total duration, and total rainfall depth are directly or indirectly used to calculate the total kinetic energy, these variables have strong correlations with the total kinetic energy. The mean maximum 30-min intensity has a strong correlation with the total rainfall depth and a low correlation with the total kinetic energy; thus, it is a good candidate as an independent variable for the R factor regression model. Many studies have provided evidence that the precipitation amount is a good independent variable in the R factor regression model (Calvo-Alvarado et al., 2014; Lee and Heo, 2011; Lee and Lin, 2015). However, when the total rainfall depth or precipitation is used for modeling the R factor, it cannot accurately represent kinetic energy and maximum 30-min intensity. In the R factor regression model using the precipitation amount, the relation between the R factor and the precipitation amount is used instead of the relations between the R factor and the kinetic energy and maximum 30-min intensity. Some studies have adapted an event-based approach or have separately modeled kinetic energy and maximum 30-min intensity for R factor modeling; these studies have reported that these approaches can perform well in modeling R factor values (Angulo-Martínez and Beguería, 2009; Richardson et al., 1983; Yin et al., 2015; Yin et al., 2007). Hence, for R factor modeling using a regression model in South Korea, the event-based approach or separate modeling of the kinetic energy and maximum 30-min intensity variables is more

Table 6
Means of the correlation matrix of the R factor and R factor-associated variables for all employed stations.

	R factor	Number of effective events	Total duration	Total rainfall depth	Max intensity mean	Total kinetic energy
R factor	1	–	–	–	–	–
The number of effective event	0.405	1	–	–	–	–
Total duration	0.449	0.815	1	–	–	–
Total rainfall depth	0.752	0.757	0.588	1	–	–
Max intensity mean	0.678	0.029	−0.025	0.653	1	–
Total kinetic energy	0.867	0.668	0.723	0.785	0.437	1

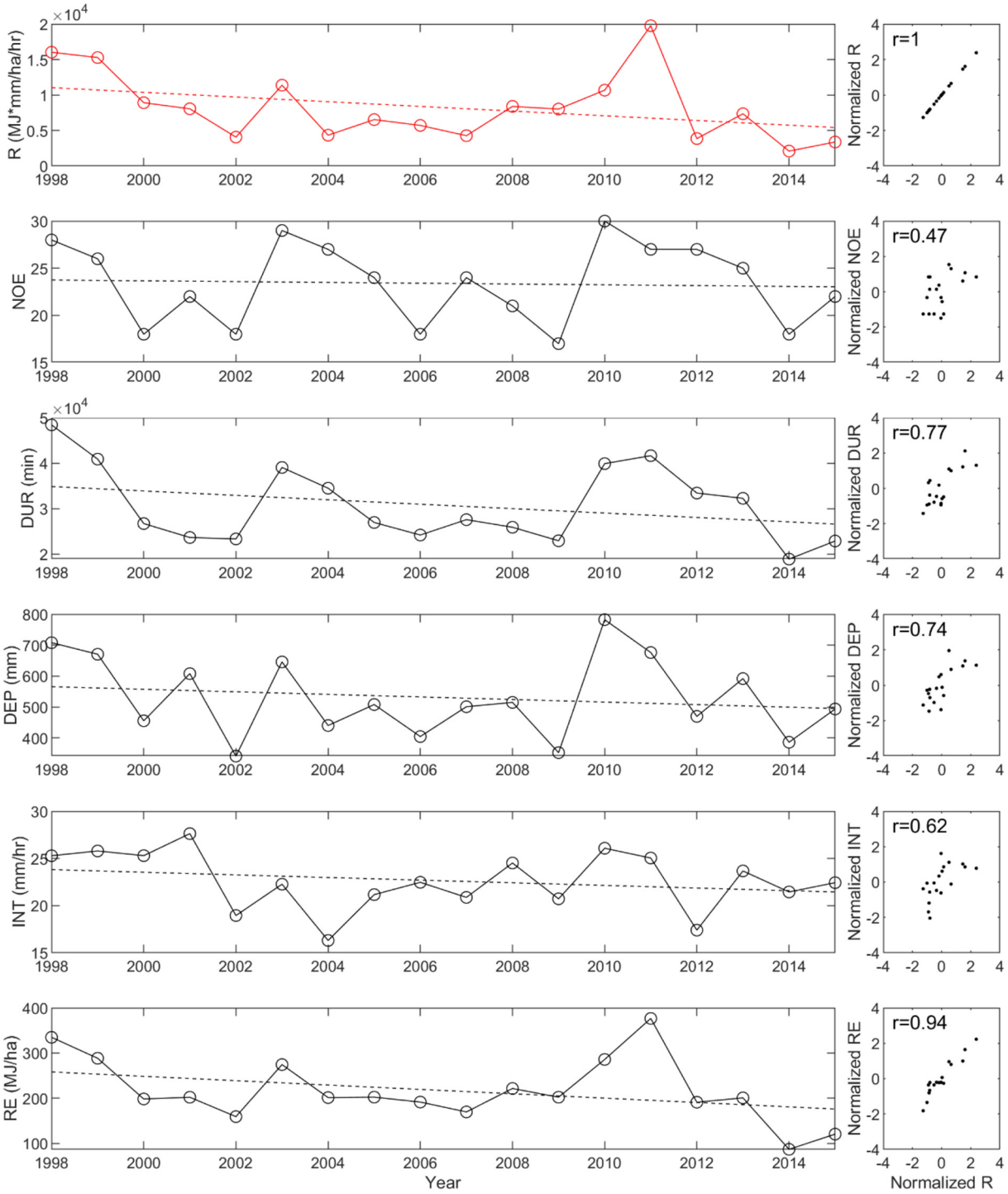

Fig. 5. Plots of time series of rainfall erosivity and rainfall erosivity-associated variables and their quantile-quantile plots for station #98 (Solid and dashed lines indicate data points and ordinary least square regression lines, respectively. Red indicates that a trend is detected in the time series of the presented variable). (For interpretation of the references to colour in this figure legend, the reader is referred to the web version of this article.)

appropriate than the regression model with precipitation.

Figs. 5 to 9 present time series plots of rainfall erosivity (R factor) and the R factor-associated variables and their quantile-quantile plots with Pearson correlation. In Figs. 5 to 9, R, NOE, DUR, DEP, INT, and RE indicate the R factor, the number of effective events, the total duration, the total rainfall depth, the mean maximum 30-min intensity, and the total kinetic energy, respectively. Based on Figs. 5 to 9, the R factor time series trends are affected by a combination of the total kinetic energy and mean maximum 30-min intensity in South Korea. Although significant trends are not detected in the maximum 30-min intensity and total kinetic energy time series, they are detected in the R factor time series. For example, as shown in Fig. 9, a significant trend is not detected in the maximum 30-min intensity and total kinetic energy time series but is detected in the R factor time series. Although increasing trends in the maximum 30-min intensity and the total rainfall depth are observed, these trends are not significant based on the 5% significant level. These weak increasing trends may lead to significant trends in the R factor time series.

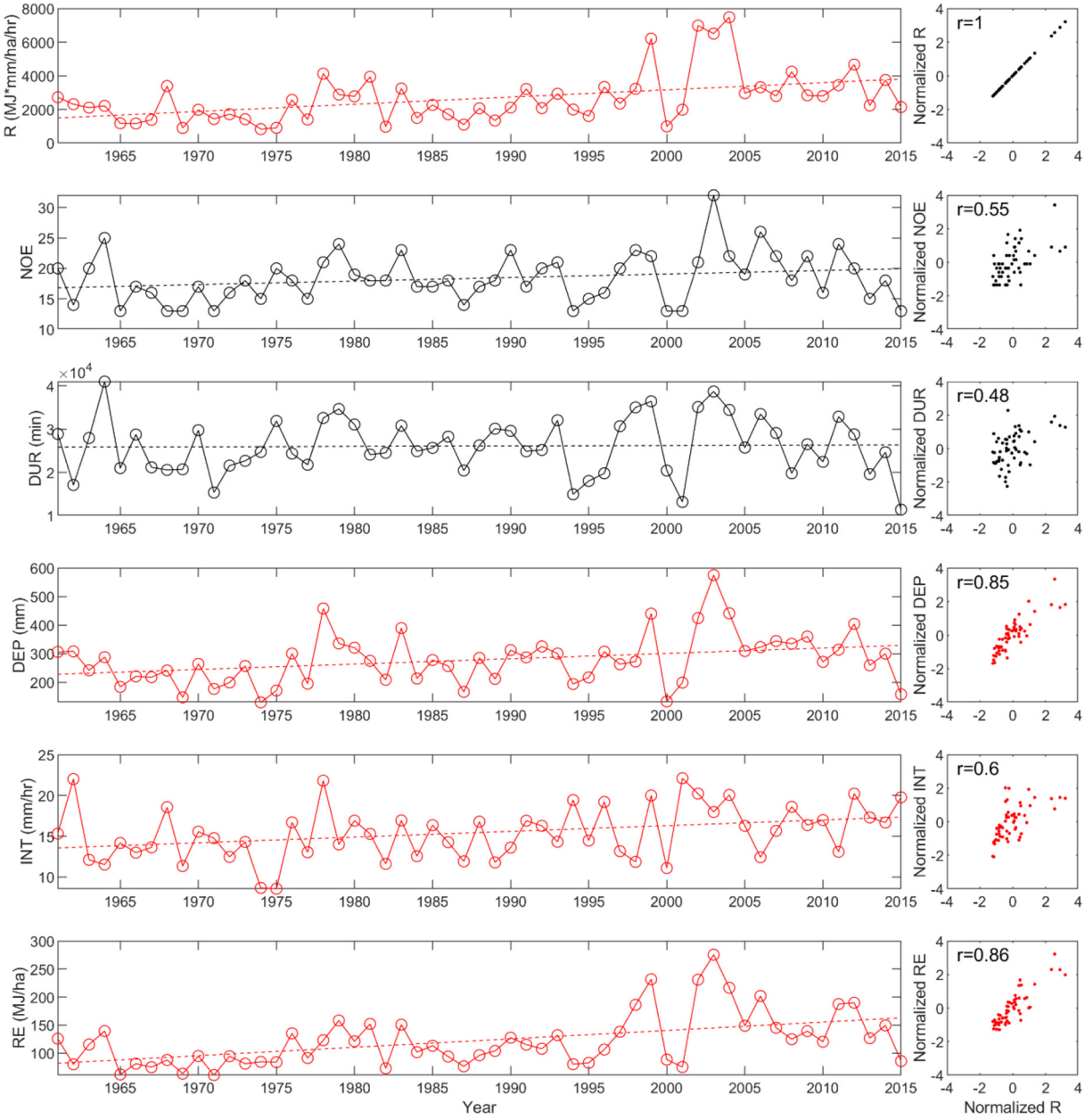

Fig. 6. Plots of time series of rainfall erosivity and rainfall erosivity-associated variables and their quantile-quantile plots for station #115 (Solid and dashed lines indicate data points and ordinary least square regression lines, respectively. Red indicates that a trend is detected in the time series of the presented variable). (For interpretation of the references to colour in this figure legend, the reader is referred to the web version of this article.)

5.2. Trends in time series of annual erosivity density

The trend tests were carried out for the erosivity density time series for all employed stations in South Korea. In all but three stations (#90, #98, and #170), the erosivity density time series do not demonstrate significant trends. The erosivity density time series are presented in Fig. 10. All detected trends are decreasing trends with very flat slopes even if their trends are significant based on the trend test results. The slope line of the erosivity density is relatively steep for station #98. Since the number of data points for the station #98 is small, the result has a large uncertainty. The results for the station #98 can be easily changed by the addition of a new data point. Thus, the results indicate that there may be no trend in the time series of erosivity density in South Korea.

6. Discussion

In the current study, the recording periods of the precipitation observation data used for the different stations are largely different. Large differences in the recording periods within the used stations can decrease the reliability of the results because nonstationary or decadal oscillation in the precipitation can lead to mean shift and trends in the data (Jung et al., 2017; Koutsoyiannis, 2006; Lee and Ouarda, 2010; Salas et al., 2018). Hence, it is necessary to investigate the impact of large differences in the recording length on estimating basic statistics of precipitation, rainfall erosivity and erosivity density. Basic statistics of precipitation, rainfall erosivity, and erosivity density for the same period (2000–2015) are calculated and presented in Appendix A.

The means for the same period are larger than the means for different periods, and their differences are small. The difference between the standard deviation for the same and different periods is very small

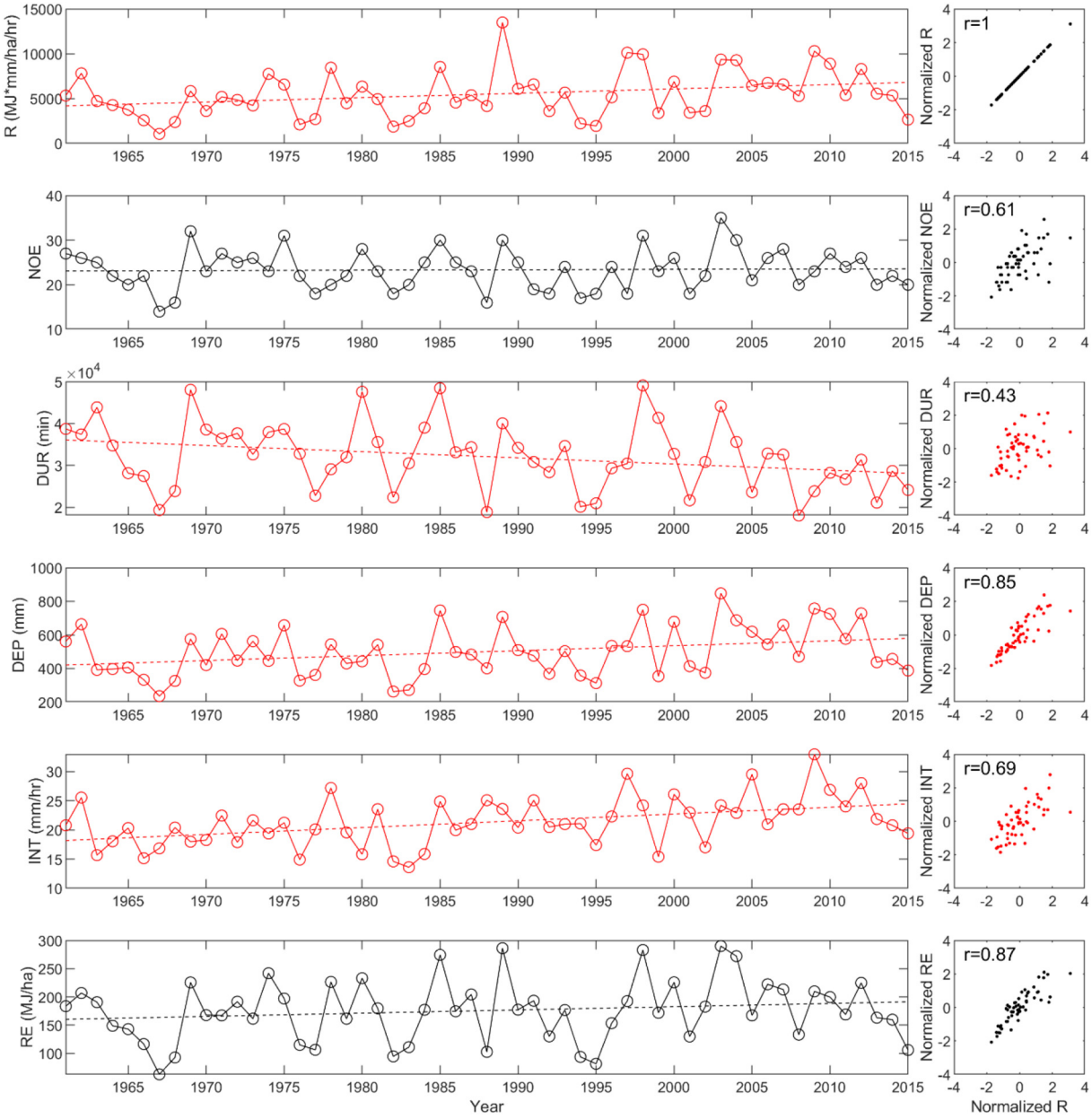

Fig. 7. Plots of time series of rainfall erosivity and rainfall erosivity-associated variables and their quantile-quantile plots for station #156 (Solid and dashed lines indicate data points and ordinary least square regression lines, respectively. Red indicates that a trend is detected in the time series of the presented variable). (For interpretation of the references to colour in this figure legend, the reader is referred to the web version of this article.)

and < 5%. Because rainfall erosivity and erosivity density are stationary or weakly nonstationary based on the trend results, the precipitation may be stationary or weakly nonstationary. Because of stationarity in data, the difference would be small. In stationary data, use of a larger number of data generally leads to more accurate and reliable estimation of the statistics. The best way to calculate and compute spatial distribution is to use the same and long recording periods for all stations. This condition is not often in the real world. To obtain the reliable estimation, using all available data would be a reasonable choice when the used data that are used are stationary or weakly nonstationary. Hence, the results in the current study would be reliable even if there are the great differences among recording periods in the different stations.

The main aim of trend tests is to investigate whether data are stationary or not. These tests allow for an examination of the time series for individual stations. Thus, to investigate trends for each station, the use of all available data would be a reasonable choice. Otherwise, to compare the trends among stations, the recording periods should be the same. In the current study, trend detection tests were carried out for two different cases: the same recording periods and different recording periods. The results of trend tests for rainfall erosivity and erosivity density are not the same but are very similar. These results indicate that the detected trends are persistent although trends are detected at only a few stations. The results of trend tests with the same periods for the total duration, total rainfall depth, and max intensity mean are different from the results with different periods while the results with the same and different recording periods for the total kinetic energy are similar. Because the *p*-values of statistics for the total duration, total rainfall depth, and max intensity mean series are close to the significance level (5%), large changes in trend test results for these variables are observed.

Kriging based spatial interpolation methods have been broadly

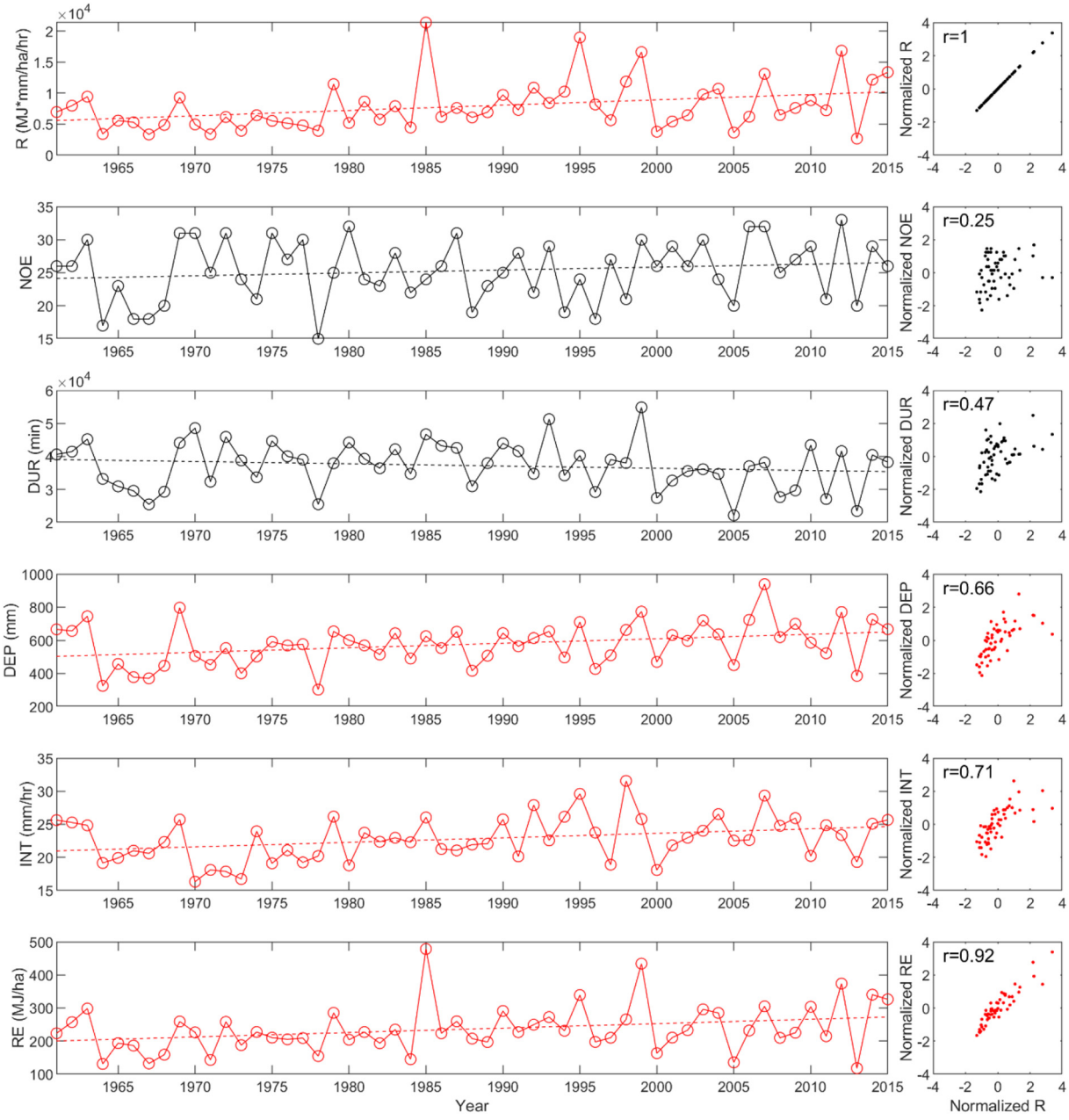

Fig. 8. Plots of time series of rainfall erosivity and rainfall erosivity-associated variables and their quantile-quantile plots for station #189 (Solid and dashed lines indicate data points and ordinary least square regression lines, respectively. Red indicates that a trend is detected in the time series of the presented variable). (For interpretation of the references to colour in this figure legend, the reader is referred to the web version of this article.)

adopted for rainfall erosivity (Borrelli et al., 2016; Lai et al., 2016; Meusburger et al., 2012; Schmidt et al., 2016). Some references recommended regression kriging for rainfall erosivity due to the high spatial variability of the rainfall erosivity. Modeling the regression kriging needs appropriate covariates such precipitation, elevation, and wind speed. Due to absences of appropriate covariate candidates, the regression kriging cannot be applied.

Thus, the applicability of an ordinary kriging scheme that does not need a covariate is tested for the spatial interpolation of precipitation, rainfall erosivity and erosivity density. The ordinary kriging method successfully provides spatial distribution of annual data. Otherwise, this method provides inaccurate results for monthly data on the September and October. For the annual and monthly erosivity density, the ordinary kriging successfully provides the spatial distribution. In the results from the ordinary kriging method, strong trends are observed in errors with the magnitude of observation. These trends indicate that the built kriging model does not use all the information in the data. These results may arise from the high spatial variability of monthly precipitation and rainfall erosivity. For example, the kriging method with the erosivity density, which has less variability than others, is working well. This high spatial variability in precipitation is shown in Fig. 2. In the current study, the IDW method is adopted as the spatial interpolation method even though the IDW is not the best method for spatial interpolation. The results of the IDW method are very similar to those of the ordinary kriging method. The spatial distribution by the IDW for the used variables may be inaccurate for regions where the network density is low.

Four trend detection tests are employed in the current study. Each trend test has advantages. To compare the performance of the trend tests for rainfall erosivity and erosivity density series, a simulation experiment has to be carried out. Although the comparison cannot be thoroughly performed in the current study, an approximate comparison

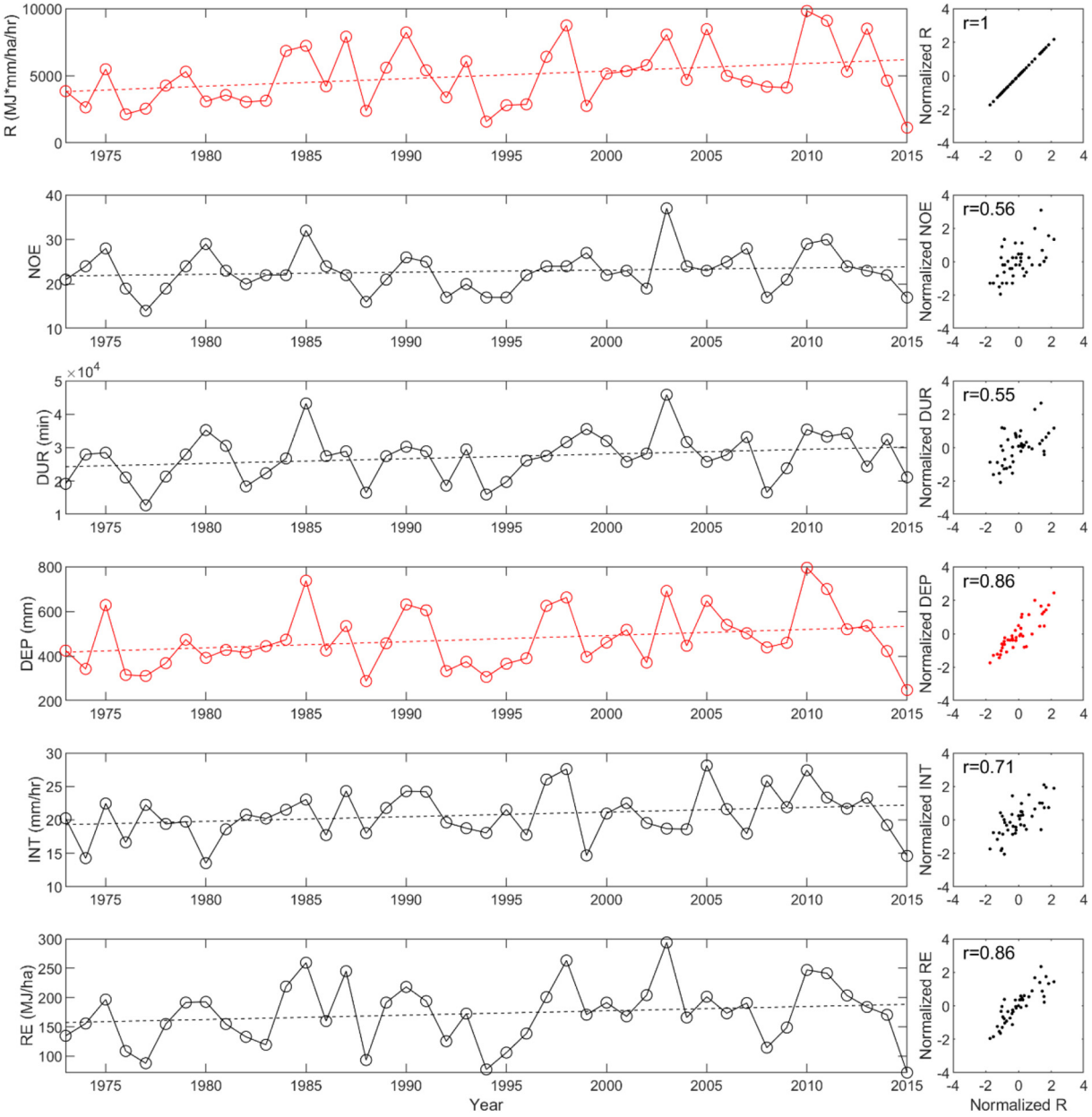

Fig. 9. Plots of time series of rainfall erosivity and rainfall erosivity-associated variables and their quantile-quantile plots for station #244 (Solid and dashed lines indicate data points and ordinary least square regression lines, respectively. Red indicates that a trend is detected in the time series of the presented variable). (For interpretation of the references to colour in this figure legend, the reader is referred to the web version of this article.)

can be deduced from the trend test results. Based on the trend test, the BBS-MK test rarely determines the presence of trends in time series of data. This result indicates that the BBS-MK test is the strictest test among the employed trend tests. Some papers reported that the BBS-MK test with appropriate simulation has higher detection power than other methods (Khaliq et al., 2009; Önöz and Bayazit, 2012). Thus, the BBS-MK test may be the most appropriate method for investigating the trend in the rainfall erosivity and erosivity density time series. The results of trend tests can change depending on the periods of the data according to the results of the trend tests for the same and different recording periods. Applying one trend detection test may lead to increased uncertainty in the trend detection. Hence, the application of a number of trend tests would be a better way to obtain reliable results of a temporal analysis for rainfall erosivity and erosivity density.

Because rainfall erosivity is a product of kinetic energy and the maximum continuous 30-min intensity, one or both variables would be critical to detect trends in rainfall erosivity. Because both variables affect rainfall erosivity trends in South Korea based on the trend test results, the trends in the rainfall erosivity can be decomposed into two components: kinetic energy and maximum intensity. The magnitude of total kinetic energy is influenced by the total rainfall depth, number of effective events, and total duration. According to the correlation matrix in Table 6, the correlation between total kinetic energy and total rainfall depth is the highest among the correlation related to total kinetic energy except for rainfall erosivity. When trends in the total kinetic energy are detected, the trends in total rainfall depth are also detected. These results suggest that the total rainfall depth may be the most critical variable influencing the trends in total kinetic energy.

7. Conclusions

The spatial and temporal variability in rainfall erosivity (R factor)

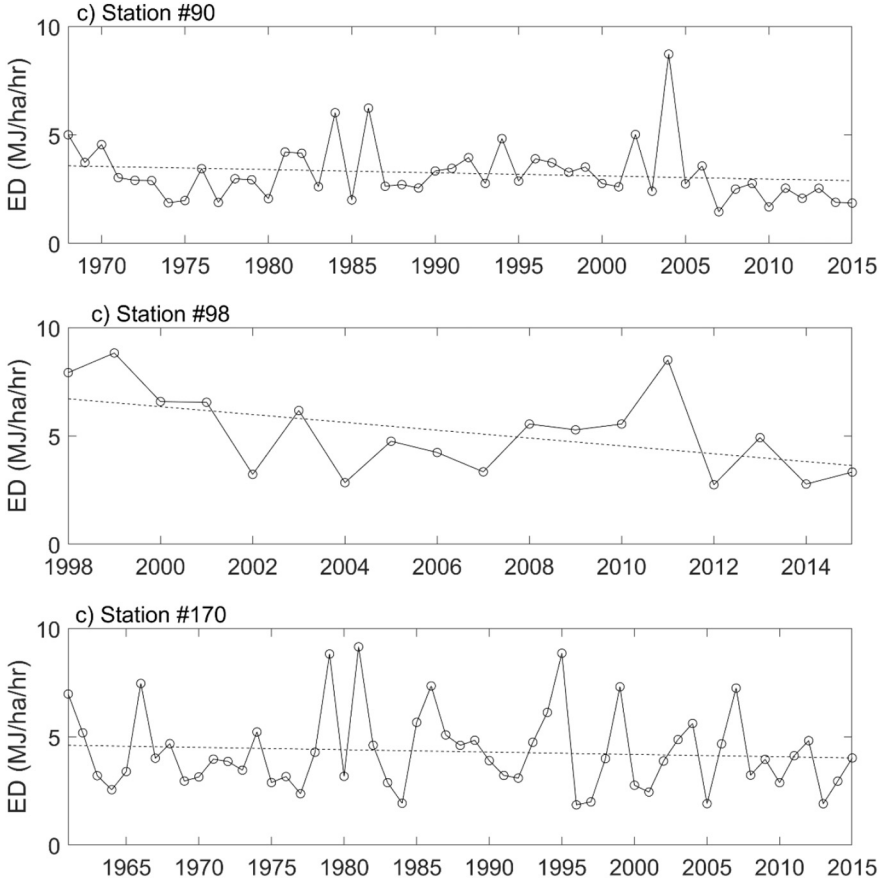

Fig. 10. Plots of time series of erosivity density means for stations #90, #98, and #244 with a trend detected by any employed trend test in the erosivity density series (Solid and dashed lines indicate data points and ordinary least square regression lines, respectively).

and erosivity density in South Korea are investigated in the present study. The annual and monthly R factors in South Korea are calculated by 5-min precipitation observations at forty-six stations in South Korea. Annual precipitation, annual R factor, and annual erosivity density spatial distributions are illustrated. In addition, this study illustrated monthly precipitation, monthly R factor, and monthly erosivity density maps. Four trend tests, i.e., the *t*-test, MK test, a modified version of the MK test, and BBS-MK test, are used to detect the trends in the annual R factor, total duration, effective event number, total depth, maximum 30-min intensity mean, and total kinetic energy time series for all employed stations. Additionally, the trends tests are carried out for the erosivity density time series in South Korea. In this study, we reach the following conclusions:

1. Annual precipitation, annual R factors, and annual erosivity density present a similar spatial pattern. Large values of annual precipitation, R factor, and erosivity density are observed in the southern coastal and northwestern regions, while small values of these factors are observed in the eastern region. The spatial variation in the annual R factor is larger than those in the annual precipitation and erosivity density.
2. In September, the R factor and erosivity density values in the northeastern region are small, even though the precipitation amount is large. In June and July, the R factor and erosivity density spatial distributions govern the annual R factor and erosivity density spatial distributions. Additionally, the spatial variation in erosivity density in June and July is small.
3. There are significant increasing trends in the annual R factor time series for five stations in South Korea. Overall, the annual R factor in South Korea does not have a significant trend. There are significant trends in the number of effective events and total kinetic energy at a few stations, while significant trends in the total duration time series are detected for many stations. The 30-min maximum intensity mean and total rainfall depth time series of ten stations in South Korea demonstrate significant trends for ten stations in South Korea.
4. Total kinetic energy and total rainfall depth are strongly correlated with the R factor in South Korea. The total kinetic energy is correlated to all the associated variables, while the maximum 30-min intensity means are correlated with the total rainfall depth. Based on correlation and graphical analyses, changes in the maximum 30-min intensity alter the R factor.

Investigating the spatial and temporal variability in the R factor of South Korea improves our understanding of rainfall erosivity, especially related to R factor characteristics in the East Asia region. R factor variability may be correlated with teleconnection or climate indices that can represent large-scale climate circulation because the long-term precipitation in South Korea has a strong correlation with climate indices (Kim et al., 2018). Further studies should investigate the relationship between the R factor and climate indices to deeply understand R factor variability in South Korea.

Acknowledgments

This work was supported by the National Research Foundation of Korea (NRF) grant funded by the Korea government (Ministry of Science, ICT & Future Planning) (No. 2015R1C1A1A02037087).

Appendix A. Basic statistics of rainfall, rainfall erosivity, and erosivity density from 2000 to 2015

Table A1
Basic statistics of annual rainfall, rainfall erosivity, and erosivity density (Note that annual rainfall, rainfall erosivity, and erosivity density are calculated from April to October).

Station code	Name	Rainfall		Rainfall erosivity		Erosivity density	
		Mean (mm)	SD (mm)	Mean (MJ·mm/ha/h/yr)	SD (MJ·mm/ha/h/yr)	Mean (MJ/ha/h)	SD (MJ/ha/h)
90	Sokcho	1442	259	4414	3107	2.95	1.75
95	Cheolwon	1394	295	6550	2737	4.54	1.28
98	Dongdocheon	1447	363	7295	4277	4.77	1.68
101	Chuncheon	1395	363	5729	2856	3.88	1.22
105	Gangneung	1456	382	5320	5068	3.27	2.26
106	Donghae	1334	343	3643	2322	2.59	1.15
108	Seoul	1469	378	8170	4533	5.25	2.15
112	Icheon	1253	300	6155	3713	4.61	2.23
114	Wonju	1378	375	6210	2944	4.32	1.19
115	Ulleungdo	1584	364	3693	1867	2.24	0.77
119	Suwon	1351	290	6344	3173	4.52	1.61
129	Seosan	1305	349	6203	4284	4.44	2.02
130	Uljin	1208	300	2926	1158	2.35	0.57
131	Cheongju	1268	310	5082	2371	3.85	1.25
133	Daejeon	1379	342	5584	2929	3.84	1.37
135	Chupungnyeong	1231	290	3594	1597	2.82	0.83
138	Pohang	1197	318	3383	1604	2.80	1.07
140	Gunsan	1312	302	5592	3009	4.05	1.56
143	Daegu	1092	253	3837	1307	3.52	1.01
152	Ulsan	1228	264	3763	1406	3.03	0.96
155	Changwon	1525	317	6534	3189	4.16	1.57
156	Gwangju	1438	272	6497	2270	4.46	1.17
159	Busan	1536	359	7001	3309	4.50	1.67
162	Tongyeong	1475	242	5763	1673	3.93	1.02
165	Mokpo	1211	227	4264	2340	3.41	1.37
168	Yoesu	1449	335	6149	2310	4.17	0.89
170	Wando	1612	315	6333	1897	3.89	0.72
184	Jeju	1505	414	6138	3586	3.83	1.42
185	Gosan	1179	246	3605	1542	2.97	0.97
189	Seogwipo	1965	483	8395	4000	4.06	1.13
192	Jinju	1567	337	6877	2766	4.25	1.18
201	Ganghwa	1274	354	6134	3335	4.56	1.60
202	Yangpyeong	1464	398	7091	3838	4.56	1.50
203	Icheon	1328	321	5571	2296	4.06	1.16
212	Inje	1390	394	6244	3414	4.30	1.59
221	Jecheon	1433	428	6178	3255	4.08	1.23
226	Boeun	1312	347	4801	2191	3.54	0.94
235	Boryeong	1216	284	5561	3406	4.28	1.92
236	Buyeo	1334	344	5454	3205	3.83	1.34
243	Buan	1285	336	5332	2733	4.10	1.58
244	Imsil	1394	287	5866	2305	4.10	1.16
245	Jeongeup	1355	270	6142	3419	4.35	1.97
248	Jangsu	1512	342	5716	2272	3.69	0.99
288	Miryang	1212	243	3970	1431	3.23	0.81
289	Sancheong	1633	387	7168	3269	4.19	1.29
295	Namhae	1878	376	9218	3490	4.83	1.31
Mean		1396	328	5685	2804	3.89	1.34

Table A2
Basic statistics of monthly rainfall, rainfall erosivity, and erosivity density in South Korea.

Variables	Statistics	Jan.	Feb.	Mar.	Apr.	May	Jun.	Jul.	Aug.	Sep.	Oct.	Nov.	Dec.
	Mean	29	41	57	98	107	151	324	281	163	56	58	32
	Proportion (%)	2.1	2.9	4.1	7.0	7.7	10.8	23.2	20.1	11.6	4.0	4.2	2.3
Rainfall	SD	22	31	36	59	56	89	173	163	127	41	47	22
(mm)	CV (%)	77	77	64	60	52	59	53	58	78	73	81	70
	CS	1.02	0.64	0.68	0.83	0.28	0.92	0.83	0.61	0.98	0.77	1.06	0.82
	CK	3.51	2.89	2.88	3.24	2.56	3.50	3.26	2.82	3.50	2.83	3.86	3.30
	Mean	21	52	64	184	265	579	2051	1707	756	142	106	23
Rainfall	Proportion (%)	0.3	0.9	1.1	3.1	4.4	9.7	34.5	28.7	12.7	2.4	1.8	0.4
erosivity	SD	37	92	76	220	249	621	1737	1527	973	191	189	39
(R factor)	CV (%)	174	177	119	120	94	107	85	89	129	134	178	168
(MJ·mm/ha/h/yr)	CS	2.18	1.65	1.67	1.72	1.19	1.49	1.15	1.22	1.75	1.51	2.02	1.73
	CK	7.23	5.34	5.87	5.88	4.23	4.84	3.95	4.27	5.83	4.66	6.74	5.57
	Mean	0.40	0.70	0.75	1.34	1.90	3.07	5.50	5.28	3.48	1.68	1.07	0.47

(*continued on next page*)

Table A2 (*continued*)

Variables	Statistics	Jan.	Feb.	Mar.	Apr.	May	Jun.	Jul.	Aug.	Sep.	Oct.	Nov.	Dec.
	Proportion (%)	1.5	2.7	2.9	5.2	7.4	12.0	21.5	20.6	13.6	6.6	4.2	1.8
Erosivity	SD	0.60	0.86	0.75	1.01	1.26	1.98	2.67	2.67	2.65	1.73	1.33	0.81
density	CV (%)	150	123	101	76	66	64	49	51	76	103	125	173
(MJ/ha/h)	CS	1.62	1.16	1.10	1.10	0.79	0.80	0.68	0.81	0.93	1.04	1.63	1.82
	CK	5.32	4.13	4.26	4.52	3.65	3.53	3.32	3.57	3.74	3.93	5.44	6.12

References

Abd Elbasit, M.A., Huang, J., Ojha, C., Yasuda, H., Adam, E.O., 2013. Spatiotemporal changes of rainfall erosivity in Loess Plateau, China. ISRN Soil Sci. 2013.

Angulo-Martínez, M., Beguería, S., 2009. Estimating rainfall erosivity from daily precipitation records: a comparison among methods using data from the Ebro Basin (NE Spain). J. Hydrol. 379, 111–121.

Aronica, G., Ferro, V., 1997. Rainfall erosivity over the Calabrian region. Hydrol. Sci. J. 42, 35–48.

Ávila, B., Ávila, H., 2015. Spatial and temporal estimation of the erosivity factor R based on daily rainfall data for the department of Atlántico, Colombia. Ingeniería e Investigación 35, 23–29.

Bae, D.H., Jung, I.W., Chang, H., 2008. Long-term trend of precipitation and runoff in Korean river basins. Hydrol. Process. 22, 2644–2656.

Baek, H.-J., Kim, M.-K., Kwon, W.-T., 2017. Observed short- and long-term changes in summer precipitation over South Korea and their links to large-scale circulation anomalies. Int. J. Climatol. 37, 972–986.

Ballabio, C., et al., 2017. Mapping monthly rainfall erosivity in Europe. Sci. Total Environ. 579, 1298–1315.

Bayley, G.V., Hammersley, J.M., 1946. The "effective" number of independent observations in an autocorrelated time series. J. R. Stat. Soc. 8, 184–197.

Beguería, S., Serrano-Notivoli, R., Tomas-Burguera, M., 2018. Computation of rainfall erosivity from daily precipitation amounts. Sci. Total Environ. 637-638, 359–373.

Biasutti, M., Seager, R., 2015. Projected changes in US rainfall erosivity. Hydrol. Earth Syst. Sci. 19, 2945–2961.

Borrelli, P., Diodato, N., Panagos, P., 2016. Rainfall erosivity in Italy: a national scale spatio-temporal assessment. Int. J. Digital Earth 9, 835–850.

Brown, L., Foster, G., 1987. Storm erosivity using idealized intensity distributions. Trans. ASAE 30, 379.

Calvo-Alvarado, J.C., Jiménez-Rodríguez, C.D., Jiménez-Salazar, V., 2014. Determining rainfall erosivity in Costa Rica: a practical approach. Mt. Res. Dev. 34, 48–55.

Cho, H.L., Jeong, J.C., 2005. Estimating soil loss in alpine farmland with RUSLE and SEDD. J. GIS Assoc. Korea 13, 79–90.

Choi, Y., 2004. Trends on temperature and precipitation extreme events in Korea. J. Korean Geogr. Soc. 39, 711–721.

D'Odorico, P., Yoo, J.C., Over, T.M., 2001. An assessment of ENSO-induced patterns of rainfall erosivity in the Southwestern United States. J. Clim. 14, 4230–4242.

Fenta, A.A., et al., 2017. Spatial distribution and temporal trends of rainfall and erosivity in the Eastern Africa region. Hydrol. Process. 31, 4555–4567.

Ferro, V., Giordano, G., Iovino, M., 2009. Isoerosivity and erosion risk map for Sicily. Hydrol. Sci. J. 36, 549–564.

Fick, S.E., Hijmans, R.J., 2017. WorldClim 2: new 1-km spatial resolution climate surfaces for global land areas. Int. J. Climatol. 37, 4302–4315.

Foster, G.R., et al., 2008. User's Reference Guide, Revised Universal Soil Loss Equation Version 2 (RUSLE-2). USDA-Agricultural Research Service, Washington, DC.

Hamed, K.H., Rao, A., 1998. A modified Mann-Kendall trend test for autocorrelated data. J. Hydrol. 204, 182–196.

Hanel, M., Máca, P., Bašta, P., Vlnas, R., Pech, P., 2016. The rainfall erosivity factor in the Czech Republic and its uncertainty. Hydrol. Earth Syst. Sci. 20, 4307–4322.

Haregeweyn, N., Yohannes, F., 2003. Testing and evaluation of the agricultural non-point source pollution model (AGNPS) on Augucho catchment, western Hararghe, Ethiopia. Agric. Ecosyst. Environ. 99, 201–212.

Haregeweyn, N., et al., 2013. Assessing the performance of a spatially distributed soil erosion and sediment delivery model (WATEM/SEDEM) in Northern Ethiopia. Land Degrad. Dev. 24, 188–204.

Hengsdijk, H., Meijerink, G., Mosugu, M., 2005. Modeling the effect of three soil and water conservation practices in Tigray, Ethiopia. Agric. Ecosyst. Environ. 105, 29–40.

Huang, J., Zhang, J., Zhang, Z., Xu, C.-Y., 2013. Spatial and temporal variations in rainfall erosivity during 1960–2005 in the Yangtze River basin. Stoch. Env. Res. Risk A. 27, 337–351.

Im, E.-S., Ahn, J.-B., Remedio, A.R., Kwon, W.-T., 2008. Sensitivity of the regional climate of East/Southeast Asia to convective parameterizations in the RegCM3 modelling system. Part 1: focus on the Korean peninsula. Int. J. Climatol. 28, 1861–1877.

Joyce, R.J., Janowiak, J.E., Arkin, P.A., Xie, P., 2004. CMORPH: a method that produces global precipitation estimates from passive microwave and infrared data at high spatial and temporal resolution. J. Hydrometeorol. 5, 487–503.

Jung, P., Ko, M., Im, J., Um, K., Choi, D., 1983. Rainfall erosion factor for estimating soil loss. J. Korean Soc. Soil Sci. Fert. 16, 112–118.

Jung, H.S., Choi, Y., Oh, J.H., Lim, G.H., 2002. Recent trends in temperature and precipitation over South Korea. Int. J. Climatol. 22, 1327–1337.

Jung, I.W., Bae, D.H., Kim, G., 2011. Recent trends of mean and extreme precipitation in Korea. Int. J. Climatol. 31, 359–370.

Jung, Y., Shin, J.-Y., Ahn, H., Heo, J.-H., 2017. The spatial and temporal structure of extreme rainfall trends in South Korea. WaterSA 9, 809.

Kang, H.S., Cha, D.H., Lee, D.K., 2005. Evaluation of the mesoscale model/land surface model (MM5/LSM) coupled model for East Asian summer monsoon simulations. J. Geophys. Res.-Atmos. 110.

Kendall, M.G., 1948. Rank Correlation Methods. C. Griffin, London.

Khaliq, M.N., Ouarda, T.B.M.J., Gachon, P., Sushama, L., St-Hilaire, A., 2009. Identification of hydrological trends in the presence of serial and cross correlations: a review of selected methods and their application to annual flow regimes of Canadian rivers. J. Hydrol. 368, 117–130.

Kim, J.-S., Jain, S., 2011. Precipitation trends over the Korean peninsula: typhoon-induced changes and a typology for characterizing climate-related risk. Environ. Res. Lett. 6, 1–6.

Kim, J., Jung, I., Park, K., Yoon, S., Lee, D., 2016. Hydrological utility and uncertainty of multi-satellite precipitation products in the mountainous region of South Korea. Remote Sens. 8, 608.

Kim, T., Shin, J.-Y., Kim, S., Heo, J.-H., 2018. Identification of relationships between climate indices and long-term precipitation in South Korea using ensemble empirical mode decomposition. J. Hydrol. 557, 726–739.

Klik, A., Haas, K., Dvorackova, A., Fuller, I.C., 2015. Spatial and temporal distribution of rainfall erosivity in New Zealand. Soil Res. 53, 815–825.

KMA, 2011. Typhoon White Book.

Koutsoyiannis, D., 2006. Nonstationarity versus scaling in hydrology. J. Hydrol. 324, 239–254.

Kwon, H., Park, G., Kim, S., 2002. Estimation of soil loss changes and sediment transport path using GIS and multi-temporal RS data. J. GIS Assoc. Korea 10, 134–147.

Lai, C., et al., 2016. Spatio-temporal variation in rainfall erosivity during 1960–2012 in the Pearl River Basin, China. Catena 137, 382–391.

Lau, K.-M., Li, M.-T., 1984. The monsoon of East Asia and its global associations—a survey. Bull. Am. Meteorol. Soc. 65, 114–125.

Le Bissonnais, Y., Montier, C., Jamagne, M., Daroussin, J., King, D., 2002. Mapping erosion risk for cultivated soil in France. Catena 46, 207–220.

Lee, J.-H., Heo, J.-H., 2011. Evaluation of estimation methods for rainfall erosivity based on annual precipitation in Korea. J. Hydrol. 409, 30–48.

Lee, G., Hwang, E., 2006. The influence analysis of GIS-based soil Erosion in water-pollutant buffering zone. J. Korean Soc. Civ. Eng. 26, 335–340.

Lee, M.-H., Lin, H.-H., 2015. Evaluation of annual rainfall erosivity index based on daily, monthly, and annual precipitation data of Rainfall Station network in southern Taiwan. Int. J. Distrib. Sens. Netw. 11.

Lee, T., Ouarda, T.B.M.J., 2010. Long-term prediction of precipitation and hydrologic extremes with nonstationary oscillation processes. J. Geophys. Res.-Atmos. 115, D13107.

Lee, S.-E., Seo, K.-H., 2013. The development of a statistical forecast model for Changma. Weather Forecast. 28, 1304–1321.

Lee, J.H., Lee, J.-h., Julien, P.Y., 2018. Global climate teleconnection with rainfall erosivity in South Korea. Catena 167, 28–43.

Li, X., Ye, X., 2018. Variability of rainfall erosivity and erosivity density in the Ganjiang River catchment, China: characteristics and influences of climate change. Atmosphere 9, 48.

Liu, S., et al., 2018. Spatial-temporal changes of rainfall erosivity in the loess plateau, China: changing patterns, causes and implications. Catena 166, 279–289.

Ma, X., He, Y., Xu, J., van Noordwijk, M., Lu, X., 2014. Spatial and temporal variation in rainfall erosivity in a Himalayan watershed. Catena 121, 248–259.

Mann, H.B., 1945. Nonparametric tests against trend. Econometrica 13, 245–259.

Matalas, N.C., Langbein, W.B., 1962. Information content of the mean. J. Geophys. Res. 67, 3441–3448.

Meddi, M., Toumi, S., Assani, A.A., 2016. Spatial and temporal variability of the rainfall erosivity factor in Northern Algeria. Arab. J. Geosci. 9, 282.

Meshesha, D.T., Tsunekawa, A., Tsubo, M., Haregeweyn, N., Adgo, E., 2015. Evaluating spatial and temporal variations of rainfall erosivity, case of Central Rift Valley of Ethiopia. Theor. Appl. Climatol. 119, 515–522.

Meusburger, K., Steel, A., Panagos, P., Montanarella, L., Alewell, C., 2012. Spatial and temporal variability of rainfall erosivity factor for Switzerland. Hydrol. Earth Syst. Sci. 16, 167–177.

Mezősi, G., Bata, T., 2016. Estimation of the changes in the rainfall erosivity in Hungary. J. Environ. Geol. 9, 43.

Millward, A.A., Mersey, J.E., 1999. Adapting the RUSLE to model soil erosion potential in a mountainous tropical watershed. Catena 38, 109–129.

Nearing, M.A., 2001. Potential changes in rainfall erosivity in the U.S. with climate change during the 21st century. J. Soil Water Conserv. 56, 229–232.

Önöz, B., Bayazit, M., 2012. Block bootstrap for Mann–Kendall trend test of serially

dependent data. Hydrol. Process. 26, 3552–3560.
Panagos, P., et al., 2015. Rainfall erosivity in Europe. Sci. Total Environ. 511, 801–814.
Panagos, P., Ballabio, C., Borrelli, P., Meusburger, K., 2016. Spatio-temporal analysis of rainfall erosivity and erosivity density in Greece. Catena 137, 161–172.
Panagos, P., et al., 2017. Towards estimates of future rainfall erosivity in Europe based on REDES and WorldClim datasets. J. Hydrol. 548, 251–262.
Pandey, A., Himanshu, S.K., Mishra, S., Singh, V.P., 2016. Physically based soil erosion and sediment yield models revisited. Catena 147, 595–620.
Park, Y.S., 2017. Development of Korean soil loss estimation model. Geoenviron. Eng. 18, 14–17.
Pontes, L.M., et al., 2017. Spatial distribution of annual and monthly rainfall erosivity in the Jaguarí River Basin. Rev. Bras. Ciênc. Solo 41.
Renard, K.G., Foster, G.A., Weesies, G.A., McCool, D.K., Yoder, D.C., 1997. Predicting Soil Erosion by Water: A Guide to Conservation Planning with the Revised Universal Soil Loss Equation (RUSLE). U.S. Department of Agriculture, Agricultural Research Service.
Richardson, C.W., Foster, G.R., Wright, D.A., 1983. Estimation of erosion index from daily rainfall amount. Trans. ASAE 26, 153.
Risal, A., et al., 2016. Application of Web ERosivity Module (WERM) for estimation of annual and monthly R factor in Korea. Catena 147, 225–237.
Sadeghi, S.H.R., Moatamednia, M., Behzadfar, M., 2011. Spatial and temporal variations in the rainfall erosivity factor in Iran. J. Agric. Sci. Technol. 13, 451–464.
Sadeghi, S.H., Zabihi, M., Vafakhah, M., Hazbavi, Z., 2017. Spatiotemporal mapping of rainfall erosivity index for different return periods in Iran. Nat. Hazards 87, 35–56.
Salas, J.D., Obeysekera, J., Vogel, R.M., 2018. Techniques for assessing water infrastructure for nonstationary extreme events: a review. Hydrol. Sci. J. 63, 325–352.
Schmidt, S., Alewell, C., Panagos, P., Meusburger, K., 2016. Regionalization of monthly rainfall erosivity patterns in Switzerland. Hydrol. Earth Syst. Sci. 20, 4359–4373.
Simpson, J., Adler, R.F., North, G.R., 1988. A proposed tropical rainfall measuring mission (TRMM) satellite. Bull. Am. Meteorol. Soc. 69, 278–295.
von Storch, H., 1999. Misuses of statistical analysis in climate research. In: von Storch, H., Navarra, A. (Eds.), Analysis of Climate Variability: Applications of Statistical Techniques Proceedings of an Autumn School Organized by the Commission of the European Community on Elba from October 30 to November 6, 1993. Springer Berlin Heidelberg, Berlin, Heidelberg, pp. 11–26.
Svensson, C., Kundzewicz, W.Z., Maurer, T., 2005. Trend detection in river flow series: 2. Flood and low-flow index series/Détection de tendance dans des séries de débit fluvial: 2. Séries d'indices de crue et d'étiage. Hydrol. Sci. J. 50, 811–824.
Van Oost, K., Govers, G., Desmet, P., 2000. Evaluating the effects of changes in landscape structure on soil erosion by water and tillage. Landsc. Ecol. 15, 577–589.
Van Rompaey, A.J., Verstraeten, G., Van Oost, K., Govers, G., Poesen, J., 2001. Modelling mean annual sediment yield using a distributed approach. Earth Surf. Process. Landf. 26, 1221–1236.
Wang, B., Ding, Q., Jhun, J.-G., 2006. Trends in Seoul (1778–2004) summer precipitation. Geophys. Res. Lett. 33.
Wischmeier, W.H., 1959. A rainfall erosion index for a universal soil-loss Equation1. Soil Sci. Soc. Am. J. 23, 246–249.
Wischmeier, W.H., Smith, D.D., 1978. Predicting Rainfall Erosion Losses - A Guide to Conservation Planning. USDA, Science and Education Administration, Hyattsville, Maryland.
Xin, Z., Yu, X., Li, Q., Lu, X.X., 2010. Spatiotemporal variation in rainfall erosivity on the Chinese Loess Plateau during the period 1956–2008. Reg. Environ. Chang. 11, 149–159.
Yin, S., Xie, Y., Nearing, M.A., Wang, C., 2007. Estimation of rainfall erosivity using 5- to 60-minute fixed-interval rainfall data from China. Catena 70, 306–312.
Yin, S., Xie, Y., Liu, B., Nearing, M.A., 2015. Rainfall erosivity estimation based on rainfall data collected over a range of temporal resolutions. Hydrol. Earth Syst. Sci. 19, 4113–4126.
Yue, S., Wang, C.Y., 2002a. Applicability of prewhitening to eliminate the influence of serial correlation on the Mann-Kendall test. Water Resour. Res. 38, 4–1-4-7.
Yue, S., Wang, C.Y., 2002b. Regional streamflow trend detection with consideration of both temporal and spatial correlation. Int. J. Climatol. 22, 933–946.
Yue, S., Wang, C., 2004. The Mann-Kendall test modified by effective sample size to detect trend in serially correlated hydrological series. Water Resour. Manag. 18, 201–218.
Yue, S., Pilon, P., Phinney, B., Cavadias, G., 2002. The influence of autocorrelation on the ability to detect trend in hydrological series. Hydrol. Process. 16, 1807–1829.